April 2015

Green Stirling Engine Power Plant

Andrew James Larsen
Worcester Polytechnic Institute

Andrew Michael Haveles
Worcester Polytechnic Institute

Beau Alexander Donnan
Worcester Polytechnic Institute

David Andrew Ephraim
Worcester Polytechnic Institute

Edward Norman Graff
Worcester Polytechnic Institute

See next page for additional authors

Author
Andrew James Larsen, Andrew Michael Haveles, Beau Alexander Donnan, David Andrew Ephraim, Edward Norman Graff, Mario Rolon, Mikhail Yuryevich Morozov, and Nathan Luis Costa

GREEN STIRLING ENGINE POWER PLANT

A Major Qualifying Project Report

Submitted to the Faculty of the

WORCESTER POLYTECHNIC INSTITUTE

in partial fulfillment of the requirements for the

Degree of Bachelor of Science

Submitted by:

Nathan Costa

Beau Donnan

David Ephraim

Edward Graff

Andrew Haveles

Andrew Larsen

Mikhail Morozov

Mario Rolón

Approved by:

Professor John Sullivan (Advisor)

Project Number: JMS-1502

April 30, 2015

Acknowledgements

Professor John Sullivan

Thanks to our advisor, Professor John Sullivan, for guiding us throughout the course of this project. His knowledge of engineering and enthusiasm for the project were essential to the group's success. The team benefited from his thoughtful recommendations and creative problem solving. He insured that project deliverables were submitted professionally and incorporated sound engineering principles.

Peter Hefti

Thanks to Peter Hefti, for keeping our lab stocked with essential equipment. He was always available for technical questions and always provided useful advice.

Manufacturing Labs Staff

Thank you to the staff in Washburn and Higgins Labs. Special thanks to Mikhail Tan and Kevin Arruda, for providing us with the proper materials, equipment, and knowledge necessary to complete this project.

Barbara Fuhrman

We would like to thank Barbara Fuhrman for her patience and assistance in the acquisition of project materials, as well as streamlining the entire MQP process.

Whitcraft LLC

Thanks to Whitcraft LLC for supplying us with the new flywheel for our engine. Team member, Edward Graff, is a Whitcraft employee and was able to acquire the material and tools necessary for the manufacturing of the flywheel.

Executive Summary

Powering our future will require replacing many of our current technologies, transforming the largest energy industries, and adopting stricter environmental policies for regulating carbon emissions. Engineers are providing economically and environmentally sustainable solutions to the energy problem that involve using renewable sources of energy, such as solar energy, for means of power generation. The purpose of this project was to develop a power plant module that was low-cost, consumer-scale, and environmentally friendly. The objective was to modify a two-cylinder auto air compression engine into an alpha-configured Stirling engine that operates using solar energy as the input thermal source. To generate electricity, the rotational motion of the crankshaft is transferred to the shaft of a permanent magnet electric generator by a simple pulley transmission.

A Stirling engine can be classified as a closed-cycle regenerative thermodynamic system that operates by cyclic compression and expansion of a working fluid at different temperatures. There are three primary configurations for a Stirling engine: the alpha, the beta, and gamma configuration. The alpha-configured Stirling engine consists of two cylinders – a hot cylinder and a cold cylinder – connected by a regenerator or mass transfer tube. Each of the cylinders contains a power piston connected to the crankshaft; the movement of the hot cylinder piston leads the cold cylinder piston by a 90-degree phase shift. The hot cylinder remains in contact with an external heat source and is maintained at high temperature. The cold cylinder, on the other hand, is maintained at low temperatures by rejecting heat through a heat exchanger. The working fluid undergoes expansion in the hot cylinder and is subsequently compressed in the cold cylinder. The work required to compress the fluid in the cold cylinder is less than that produced by expansion in the hot cylinder, resulting in a positive net work output. The Stirling

cycle will continue as long as the temperature differential between the cylinders creates sufficient energy to overcome the internal friction of the engine. For the purposes of this project, an alpha-type Stirling engine was chosen using solar energy as the heating source.

To investigate the feasibility of green power sources for the Stirling engine, a parabolic dish was constructed using a wooden frame, a Mylar emergency blanket for a reflector, and caulking sealant. A vacuum could be drawn through a ball valve, which stretched the Mylar inwards to form a parabolic reflecting surface. The parabolic Mylar surface serves as a solar collector and is designed to concentrate solar energy at a specific focal point dictated by the curvature of the mirror, and thus, the strength of the vacuum. With the focus adjusted by altering the internal pressure, incoming solar energy was directed onto a black aluminum target plate and its temperature measured via thermocouple. The temperature was then used to calculate the total power reflected by the dish.

The maximum temperatures and power extrapolations obtained from the solar test prompted the design of a motorized, automated mount capable of both elevation and azimuth adjustments over time. This allows for easy maintenance of the reflector as it would no longer need to be aimed by human operators. The dish mount was constructed from wood and could pivot about its center on four wheels to satisfy tracking capabilities.

Extensive modifications and improvements were performed on the existing engine. New cylinder heads, mass transfer tube, and flywheel were designed and manufactured. In addition, the crankshaft was ground down to install a needle bearing to reduce internal friction. New gaskets were fabricated from temperature resistant materials. A valve was also added to enable pressurization of the working fluid. Although the internal friction was reduced by nearly 90 percent, the engine was not able to sustain its thermodynamic cycle.

The engine was connected to an electrical power generation system by a V-belt drive transmission. The electrical infrastructure consisted of a Windzilla permanent magnet DC generator for power generation, a Xantrex C35 charge controller for regulating voltage and current, a Scorpion 12V absorbed glass mat battery for power storage, and a 1kW 1Ohm resistor as a diversion load. The engine and all electrical components were housed in a custom built steel frame.

By the conclusion of the project, a solar collection system and electric power generation system were designed, fabricated, and tested. The engine modifications to reduce internal friction and dead volume were successful; however, these improvements were not enough to sustain cyclic operation of the engine.

Abstract

The Green Stirling Engine Power Plant project utilized a Stirling engine as an environmentally responsible means of electrical power generation. The team's efforts centered on A) collecting solar energy through a parabolic mirror to transmit that energy to B) an adapted two-cylinder compressor engine, which served as a repurposed Stirling engine and C) convert the engine's power to electricity through a DC generator and battery storage. To realize these efforts the available solar energy was calculated and a prototype parabolic mirror was designed, constructed and tested. The engine was modified to serve as an Alpha-Stirling design, which was mounted in a test apparatus containing the DC generator, battery storage, and a charge controller. It was necessary to design numerous engine components including the cylinder heating and cooling heads, a mass transfer tube, a crankshaft, and flywheel. The DC generator and charging system was tested and shown to produce the required electrical outputs. Overcharging the battery was prevented through the use of the charge controller and a large resistive diversion load.

Contents

List of Figures

List of Tables

Chapter 1: Introduction

In the technological world of today, the need for power is ever-growing. With the increasing concern of global warming and the harm fossil fuel power sources cause the world, the search for green power is necessary. A problem with environmentally friendly power sources is their cost (Your Guide to Renewable Energy, n.d.). Engineers today must look for solutions that are economically viable as well as environmentally friendly.

A potential solution to both of these problems is the Stirling engine. Operating costs are reduced in the case of Stirling engines since they have no internal combustion and typically only use air as the working fluid as opposed to fuel and air mixes. The problem, however, is acquiring a heat source potent enough to heat the engine to the required temperatures and be both economically and environmentally feasible. Furthermore, Stirling engines are yet to be widely used and commercially available.

The present project served to design, construct, and test a green Stirling engine power plant. The purpose of the project was to examine the feasibility of having a Stirling engine be powered with a green energy source in order to produce mechanical energy in a more environmentally friendly way.

Chapter 2: Background

To understand the working principle of the Stirling engine, the distinction between Stirling engines and other types of heat engines must be clearly stated. A heat engine is a thermodynamic system that converts heat or thermal energy to mechanical energy, which can then be used to do mechanical work. Internal combustion engines and external combustion engines are two distinct families of heat engines that generate mechanical power by the combustion of a fuel in the presence of an oxidizer. Automobile engines and gas turbines are the classic examples of internal combustion engines, both of which rely on the work done by expanding gases in the combustion chamber (or in the case of gas turbines, the combustor). The steam engine, on the other hand, is a prime example of an external combustion engine, whereby the fuel (typically coal or wood) is combusted outside of a sealed boiler containing the moving gases - in this case, steam. The thermal energy produced by the combusting fuel serves as the primary source of energy in the case of both internal and external combustion engines. Conversion of the thermal energy into mechanical work is typically achieved via the rotation of a shaft. This shaft rotation can be used to power a variety of machines from automobiles to passenger aircraft to water pumps.

The internal combustion engine is a heat engine in which the mixing of fuel and oxidizer occurs in a confined space called a combustion chamber. The resulting exothermic reaction between the fuel and oxidizer (typically air) creates gases of high temperature and pressure, which are permitted to expand in the chamber. The defining feature of an internal combustion engine is that useful work is performed by the expanding gases acting directly to cause movement, for example by acting on pistons in an automotive engine or rotor blades in a gas

turbine. The cycle is maintained by cyclic combustion events inside the combustion chamber, and the fuel and oxidizer must be resupplied at each of these events.

In contrast to the internal combustion engine, the external combustion engine (i.e. steam engine) uses the combustion process to heat a separate working fluid. The working fluid absorbs the input thermal energy from the combustion event through a heat exchanger, which upon expansion, does work on some internalized mechanism, for example by pressing on a steam actuated piston. The working fluid in an external combustion engine is brought to high pressures by the external thermal source, whether it is through the engine wall or another type of heat exchanger. The fluid then, by expanding and acting on the mechanism of the engine, produces rotational motion and usable work. Subsequently, the fluid is cooled, compressed, and reused (closed cycle). This cycle is maintained as long as the external thermal source remains in contact with the heat exchanger.

Similar to the steam engine, the Stirling engine can be traditionally classified as an external combustion engine, as all heat transfers to and from the working fluid takes place through a heat exchanger (usually through the cylinder walls or heads), thus isolating the combustion process and any contaminants it may produce from the working parts of the engine. The Stirling engine uses a fixed amount of working fluid (typically pressurized air) enclosed in a sealed volume, and the heat consumed by the engine is applied externally. This allows the engine to operate using any heat source including fossil fuels, hot air, solar, chemical, and nuclear energy. The thermodynamics of the Stirling cycle is independent of the type of heat source since it is supplied externally.

2.1 History of the Stirling Engine

The Stirling engine was first developed and patented by Robert Stirling in Edinburgh, Scotland in 1816. Stirling proposed an engine design that operated by cyclic compression and expansion of a gaseous working fluid at different temperatures, such that there is a net conversion of heat energy to mechanical work (Thombare & Verma, 2008). Unlike internal combustion engines, the Stirling engine is a closed-cycle (as opposed to an open-cycle) regenerative heat engine containing a fixed amount of gaseous working fluid in an airtight volume. Internal combustion engines, such as those in automobiles, have intake and exhaust valves that are continuously opening and closing to recycle the working fluid, and thus, are classified as open cycle systems. The term *closed-cycle* in this context simply refers to a thermodynamic system in which the working fluid is permanently contained within the system, and *regenerative* describes the use of a specific type of internal heat exchanger and thermal store.

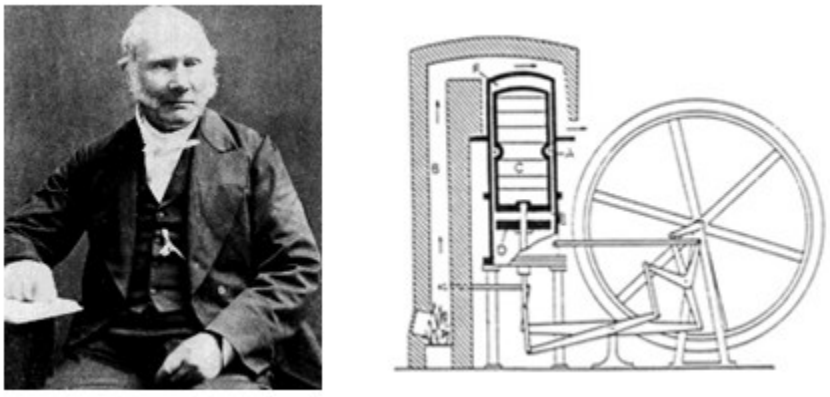

Figure 1 Robert Stirling (left) and his proposed heat engine design (right) (Stirling International, 2015)

By trade, Robert Stirling was a minister in the Church of Scotland and continued to provide religious services to those in his community until he was eighty-six years old. In his

spare time, Stirling built heat engines in his home workshop with his younger brother James - an engineer. At the time of its conception, the Stirling engine was considered to be a promising replacement to the steam engine. This was partly because the boilers used in early steam engines were prone to explosion due to the high pressures exerted by the expanding vapors. Stirling sought to create a safer alternative to the steam engine by eliminating the need for internally combusting gases and relying solely on temperature differentials between regions of cold and hot air.

The main subject of Robert Stirling's original patent was a heat exchanger, which he called an *economizer* for its enhancement of fuel economy in a variety of applications. The patent also described in detail the employment of one form of the economizer in his unique closed-cycle air engine design; this form of the economizer is now generally referred to as a regenerator. A schematic of Stirling's proposed heat engine is provided in Figure 1. The inclusion of a regenerator certainly differentiates the Stirling engine from other closed cycle hot air engines. The regenerator in the Stirling engine absorbs heat from the working gas when the gas flows from the hot region to the cold region, and releases heat during the reverse process (Minassions, 2007). The Stirling engine can obtain higher thermal efficiencies than traditional combustion engines due to the presence of the regenerator. A measure of Stirling's perceptive genius can be discerned from the fact that it was not until in 1850, following the introduction of Joule's concept of the mechanical equivalent of heat, that William Rankine was able to explain satisfactorily the operation of a Stirling engine (Walker & Senft, 1985).

Originally conceived as an industrial prime mover to rival the steam engine, its practical use was largely confined to low-power domestic applications. The Stirling engine was first used in 1818 as a pumping device to push water in a quarry, and continues to be used for water

pumping projects in rural areas (Bumataria & Patel, 2013). Subsequent development by Stirling and his brother James resulted in patents for various improved configurations of the original engine including pressurization, which by 1843, had sufficiently increased power output to drive all the machinery at a Dundee iron foundry (Jadhao & Mahantare, 2013). However, the need for Stirling engines to run at extremely high temperatures to maximize power and efficiency exposed limitations in the materials of the day, and the few engines that were built in those early years suffered unacceptably frequent failures (albeit with far less disastrous consequences than the boiler explosions common to steam engines). The Stirling engine used at the Dundee foundry was eventually replaced by a steam engine after three hot cylinder failures in four years (Finkelstein & Organ, 2010). Although the Stirling ultimately failed as a competitor to the steam engine, during the late nineteenth and early twentieth centuries, smaller hot air engines were produced in large numbers, finding niches wherever a reliable source of low to medium power was required, most notably for raising water. These generally operated at lower temperatures so as not to tax available materials and thus tended to be rather inefficient; their major selling point, in contrast to the steam engine, was that they could be operated safely by anybody capable of managing a fire. As the century progressed, this role was eventually usurped by the electric motor and small internal combustion engines, and by the late 1930s, the Stirling engine was a largely forgotten scientific curiosity represented only by toys and a few small ventilating fans (Stirlingshop.com, n.d.).

The name *Stirling engine* was officially coined nearly one hundred years after its conception by a Dutch engineer Rolf Meijer to describe all types of closed-cycle regenerative gas engines. It was suggested by Fleeming Jenkin as early as 1884 that all regenerative heat engines should generically be referred to as *Stirling engines*. This naming proposal found little favor at

the time, and the various engine types on the market continued to carry the name of their respective designers or manufacturers including Rider's, Robinson's, and Heinrici's hot air engines (Wikipedia, n.d.). In the 1940s, the Philips Company was seeking a suitable name for its own version of a hot air engine, which by that time had been tested with working fluids other than air, and officially decided upon *Stirling engine* in April 1945. However, nearly thirty years later, Graham Walker still had cause to bemoan the fact such terms as *hot air engine* remained interchangeable with *Stirling engine*, which itself was applied widely and indiscriminately (Walker & Senft, 1985).

All Stirling engines require that a temperature differential be maintained between the hot and cold regions of the engine to ensure that work done by the moving gases can overcome the internal frictional forces acting on the crankshaft. Early in 1983, Professor Ivo Kolin of the University of Zagreb, Croatia, successfully demonstrated the very first low temperature differential Stirling engine (Vineeth C.S., 2012). This engine operated on a temperature difference of 100°C, which at the time was an astonishingly low temperature differential. Professor Kolin and his colleagues developed a series of hot air engines exploring the minimum temperature differential needed to maintain cyclic expansion and compression of the working fluid. Fortunately they were able to reduce the temperature differential to a nearly 20^{o}C. This feat was all the more remarkable considering that their engines were constructed entirely with hand tools. The engine had no power piston and cylinder; instead, it relied on a rubber diaphragm to transmit the power from the square main chamber. A distinct feature of this engine was the *slip-link* - a mechanism for imparting intermittent motion to the displacer piston inside the main chamber. At low speeds, a dwell at both top dead center and bottom dead center of the displacer stroke was proved to be favorable (Vineeth C. S., 2012). Professor Kolin continued to refine his

low temperature engines using the diaphragm, but simplified the original displacer drive mechanisms.

Beginning in the late 1980s, Professor Senft of the University of Wisconsin tackled the idea of low temperature differential Stirling engines. The first models Senft produced were Ringbom engines; these engines had no direct mechanical connection between the flywheel and the displacer (Vineeth C.S., 2012). Pressure changes inside the engine caused by the movement of the power piston act on an oversized displacer pushrod to create movement of the displacer piston. Professor Senft was asked to design and build a low temperature differential engine for North American Space Association (NASA). This engine, called the N-92, was optimized for handheld operation, with a temperature difference as low as 6°C. Professor Senft continues to work with Stirling engines, and has written several books detailing the history and manufacture of hot air engines.

Stirling engine enthusiast Andy Ross has also contributed a number of design solutions for increasing the operating efficiencies of Stirling engines. By December of 1976, Ross devised the yoke drive mechanism for the two piston Stirling engine, now generally referred to in literature as the *Ross linkage,* which permits the use of a single crankpin and eliminates side forces on the pistons (Ross, 1993). The yoke drive consists of a triangular yoke mounted on a single crankpin, and guided by a rocking lever. The combination of the circular motion of the crankpin and the arc of the rocking lever produces nearly linear motion at the extended arms of the yoke, with a phase between the motion very suitable for a two piston Stirling engine. The three major advantages of this drive mechanism are: (1) very low piston side loads, permitting long life and low friction with oil-less operation, (2) closely spaced parallel cylinders, which are

easily connected with compact heat exchangers, and (3) relatively small size and low weight for a given swept volume (Ross, 1993).

2.1.1 Working Principle of the Stirling Engine

The Stirling engine is perhaps the simplest form of engine in terms of working principle. Unlike internal combustion engines, the Stirling cycle proper is an ideal thermodynamic cycle consisting of two isothermal (constant temperature) and two isometric (constant volume) regenerative processes as shown on the pressure-volume and temperature-entropy diagrams in Figure 2. Closed regenerative thermodynamic cycles, like the Stirling cycle, rely on heat regeneration following compression of the working fluid to increase overall thermal efficiency (and approach the Carnot efficiency). Gas is used as the working fluid in most cases, and undergoes cyclic compression and expansion in separate chambers of the engine.

To illustrate the sequence of operations, consider a cylinder containing two opposed pistons with a regenerator between the two pistons. The thermal regenerator is a form of heat exchanger acting as a thermodynamic sponge that alternately accepts and rejects heat to and from the working fluid, thus recycling a large fraction of the energy flow from one cycle to the next (Walker & Senft, 1985). One of the two volumes between the regenerator and the piston heads is called the *expansion space*, and is maintained at a high temperature by means of external combustion or some other source of thermal energy. The other volume is called the *compression space,* and is maintained at a low temperature. The temperature differential that exists between the expansion space and the compression space gives rise to a temperature gradient across the transverse faces of the regenerator. It is assumed that there is no thermal conduction in the longitudinal direction, and that the pistons move without friction or leakage loss of the working fluid enclosed. However, internal frictional forces on the crankshaft and leakage of the working

fluid both contribute to the difficulties in maintaining cyclic compression and expansion in the cylinders. For the sake of the thermodynamic analysis, the effects of friction and fluid leakage can be neglected.

To start the cycle, heat must first be applied to the engine head of the *hot cylinder*; subsequent conduction through the hot head and convection into the expansion space causes the pressure of the working fluid in the hot cylinder to increase, pushing the power piston downwards. The downward movement of the power piston prompts upward movement of the displacer piston in the neighboring cylinder - the *cold cylinder.* As the power piston completes its downward stroke and the expansion space volume is maximized, the displacer piston reaches the end of its upward stroke and the compression space volume is minimized (zero). Assuming that the rotational inertia of the crank is sufficient to reverse piston motion, the upward stroke of the power piston forces the high-temperature air out of the hot cylinder, through the regenerator, and into the cold cylinder. Thermal energy is extracted from the working fluid and stored in the regenerator when the gas is flowing from the hot cylinder to the cold cylinder. The temperature of the working fluid is reduced to that of the cold source, and the pressure of the air decreases as a result. At this stage, all of the working fluid is in the cold compression space and the volume is at a maximum, thus the temperature and pressure are minimum values. As the displacer piston proceeds through its upstroke and the volume of the compression space decreases, the working fluid in the cold cylinder is compressed and the pressure increases. The temperature, however, is maintained constant because heat is abstracted from the compression space into the surroundings. Fins are often machined into the engine head of the cold cylinder to control the heat abstraction during compression (Walker & Senft, 1985). Following the compression stage,

the gas flows back into the expansion space and absorbs heat energy from the regenerator along the way.

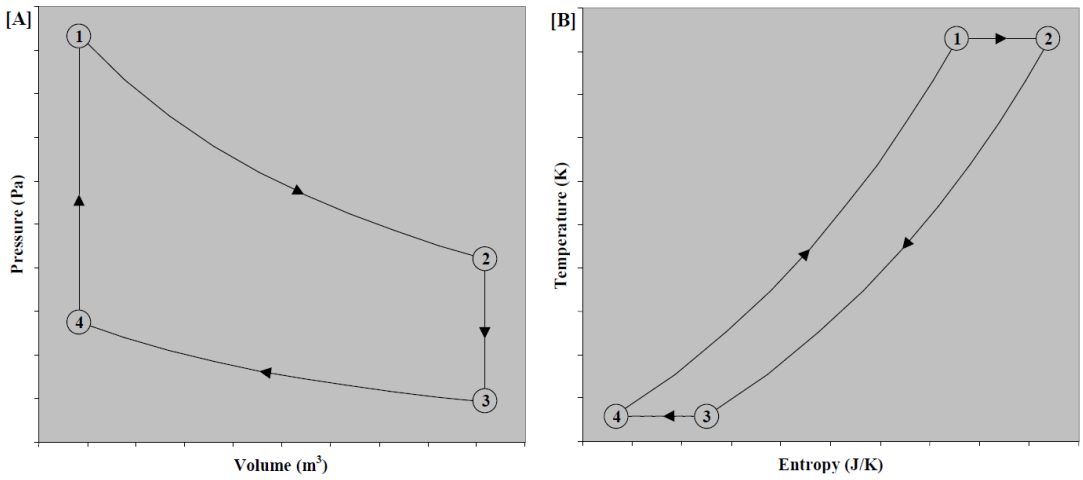

Figure 2 (A) Pressure-volume and (B) temperature-entropy diagrams for an ideal Stirling engine

The stages of the ideal Stirling cycle, as labeled in *P-V* and *T-S* plots in Figure 2, can be summarized as follows:

Stage 1 – 2: Isothermal (constant temperature) expansion – the working fluid in the expansion space absorbs heat energy form an external source and expands isothermally, thus doing work on the power piston.

Stage 2 – 3: Isochoric (constant volume) displacement – the displacer piston transfers all the working gas isochorically through the regenerator to the cold cylinder. Heat energy is extracted from the gas to the regenerative matrix as it passes from the cold cylinder to the hot cylinder. The temperature of the gas is reduced to that of the cold source; consequently, the pressure also decreases.

Stage 3 – 4: Isothermal compression – the displacer (or in some cases, the power piston) does work on the gas and compresses it isothermally in the cold cylinder. The heat energy produced from compression of the working fluid in the compression space is rejected into the surroundings via a heat exchanger. Since the gas is at lower pressure, less work is required for compression than was obtained from the gas during expansion (in stage 1 - 2); therefore, the cycle has a net work output.

Stage 4 – 1: Isochoric displacement – the displacer piston transfers all the working gas isochorically through the regenerator to the hot cylinder. Heat is delivered to the gas as it passes through the regenerator, thus raising the temperature of the gas to that of the expansion space. As the temperature rises, the gas pressure increases significantly, and the system returns to its initial conditions.

2.1.2 Stirling Engine Configurations

There are essentially three types of Stirling engines that are distinguished by the way in which the working fluid is transferred between the hot and cold regions of the engine. The *alpha* configuration of the Stirling consists of two power pistons, one in the hot cylinder, and the other in the cold cylinder; the gaseous working fluid is driven between the two cylinders by the moving pistons. The hot and cold cylinders of an alpha Stirling engine are typically in a V-formation with the power pistons joined at the same point on a crankshaft and aligned at 90 degrees relative to each other. The *beta* configuration of the Stirling has a single cylinder with a hot end and a cold end, containing a power piston and a displacer piston that drives the gas between these two regions. It is typically used with a rhombic drive to achieve the phase difference between the displacer and power pistons, but the pistons can be joined 90 degrees out of phase on a crankshaft. Lastly, the *gamma* configuration has two cylinders: one containing a

displacer, with a hot and a cold end, and one containing the power piston. The pistons are joined to form a single space with equal pressure in both cylinders; the pistons are typically in parallel and joined 90 degrees out of phase on a crankshaft.

As stated previously, an *alpha* Stirling contains two power pistons and two cylinders (hot and cold) connected via a regenerator. The hot cylinder is situated inside the high temperature heat exchanger while the cold cylinder is in contact with the low temperature reservoir, which in many practical applications is the atmosphere. The two pistons are connected to a flywheel in such a way that the linear, translating motion of the power pistons can be converted into rotary motion and the phase difference can be maintained. This type of engine has a high power-to-volume ratio, but has technical problems due to the high temperature of the hot piston and the durability of its seals (Vineeth C.S., 2012). High temperatures can cause the piston to expand and increase the internal frictional forces between the piston and cylinder walls. The stages of the alpha Stirling cycle are illustrated in Figure 3. Initially, the working fluid is heated by the high temperature heat exchanger and expansion of the gas pushes the hot piston to the lowest point of its downstroke. The hot cylinder piston then moves most of the heated gas into the cold cylinder; at this stage, the air begins to cool and the pressure is decreased. The cold piston, powered by flywheel momentum, compresses the gas in the cold cylinder and heat is rejected through the low-temperature heat exchanger. The working fluid is pushed back into the hot cylinder by the cold cylinder piston, undergoes expansion upon heating, and drives the hot cylinder piston into its power stroke once again (Jadhao & Mahantare, 2013).

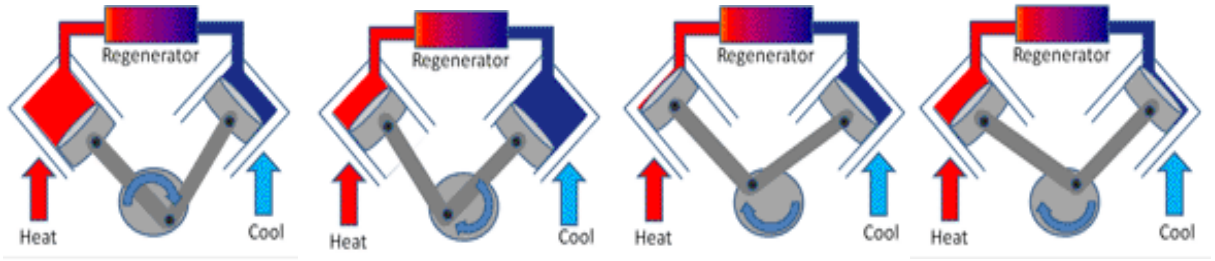

Figure 3 Operation of the alpha configured Stirling engine, from left to right (Electropaedia, n.d.)

The thermodynamics of the Stirling *beta* engine are similar to those of the *alpha* engine, but the physical configuration of the engine components is quite different. Unlike the two-cylinder alpha configured Stirling engine, the *beta* engine is relatively compact and is comprised of only single cylinder with a heated end and a cooled end. A power piston is arranged coaxially in the cylinder along with a displacer. The displacer piston does not extract any power from the expanding gas but only serves to shuttle the working gas back and forth between the hot and cold ends. The purpose of the power piston is to generate power, while the purpose of the displacer is to move the working fluid back and forth through the heated region, regenerator, and cooled region. As a result, the pushing force experienced by the displacer is very little compared to that of the power piston. As in the *alpha* engine, the cyclic motions of the pistons are 90 degrees apart with the motion of the displacer piston leading the power piston by a quarter revolution of the crankshaft.

The power piston, displacer, and displacer rod in the beta engine are sealed around their gaps to prevent the leakage of working gas. The seal for the displacer is placed on the end closest to the compression space, in order to avoid direct contact with the hot working gas (in the expansion space). As a result, this seal does not need to be temperature resistant. The seals for the displacer rod and power piston do not need to be temperature resistant either since they are constantly exposed to cool engine temperatures. This is due to their physical proximity to the

compression space (Electropaedia, 2015). Figure 4 illustrates the beta configured Stirling engine and the cyclic motions of the displacer and power piston.

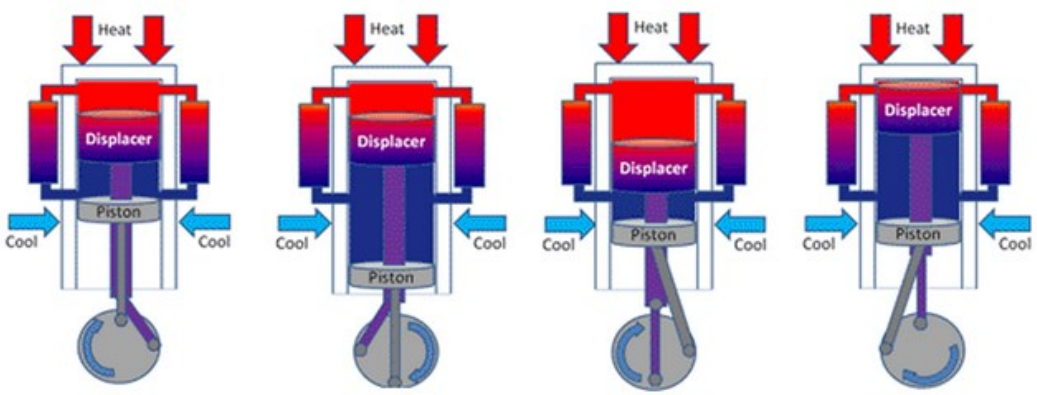

Figure 4 Operation of the beta configured Stirling engine (Electropedia, n.d.)

A disadvantage of the beta engine is that it can be difficult to minimize the dead (clearance) volume in the expansion and compression space, given that there must be enough clearance to allow the working gas to flow unobstructed from the hot region and the cold region.

Lastly, the Stirling *gamma* configuration is simply a Stirling beta engine in which the power piston is not mounted coaxially with the displacer piston but in a separate cylinder. This avoids the complications of the of the displacer piston linkage passing through the power piston. A fixed amount of working fluid is maintained within the cylinders by the pistons, which form a gas tight seal with the cylinder walls. The displacer is a loose fit within the hot cylinder, allowing the gas to pass down the sides as it moves up and down. As with other Stirling engines, the gas is alternately heated and cooled causing it to expand and contract as it shuttles between the hot and cold cylinders transferring its energy to the power piston in the cold cylinder. A disadvantage of the gamma engine is that it unavoidably introduces dead volume in the compression space due to the physical separation of the displacer and power piston. Figure 5 shows the layout of the gamma configured Stirling engine.

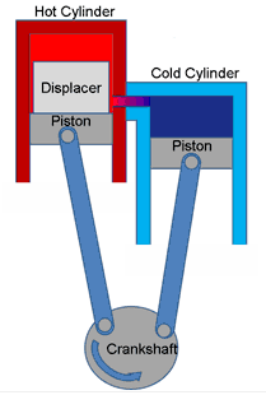

Figure 5 Gamma configured Stirling Engine (Electropedia, n.d.)

The three basic types of Stirling engines described previously might employ a wide assortment of crank drive mechanisms or none at all, as in free piston Stirling engines. The main requirements for successful operation are high mechanical efficiency and simplicity, with other important considerations including good dynamic balance, the ability to operate with minimal lubrication, and compactness.

2.1.3 Modern Applications of the Stirling Engine

Stirling engines are able to run on virtually any source of heat, even at relatively low levels. They are known to operate more efficiently than gas or diesel-fueled engines. Stirling engines can also serve as sources of clean energy, but have only been used in specialized, small niche applications. Although today the Stirling engine is most commonly used to power submarines, auxiliary power generators, large scale solar power, or as small models and toys, they have the potential to be developed for commercial use in a much larger market if the proper research and testing is conducted (Kontax, n.d.).

It is often claimed that the Stirling engine has too low a power/weight ratio, too high a cost, and too long a starting time for automotive applications. They also have complex and expensive heat exchangers. In fact, a Stirling cooler (or cold cylinder) must reject twice as much

heat energy as an Otto engine or diesel engine radiator (Mathas, 2014). The heater must be manufactured from stainless steel, ceramic, or an exotic alloy to support high heater temperatures needed for high power density, and to contain hydrogen gas that is often used in automotive Stirling engines to maximize power. Hydrogen gas is often used in automotive Stirling engines due to its high thermal conductivity and low viscosity. The major difficulties involved in using the Stirling engine in an automotive application are startup time, acceleration response, shutdown time, and weight, not all of which have ready-made solutions. However, a modified Stirling engine has been introduced that uses concepts taken from a patented internal-combustion engine with a sidewall combustion chamber that promises to overcome the deficient power-density and specific-power problems, as well as the slow acceleration-response problem inherent in all Stirling engines (Hacsi, 2008). It could be possible to use these in co-generation systems that use waste heat from a conventional piston or gas turbine engine's exhaust and use this either to power the ancillaries (i.e. an alternator) or even as a turbo-compound system that adds power and torque to the crankshaft (Wikipedia, n.d.). Automobiles exclusively powered by Stirling engines were developed in test projects by NASA, as well as earlier projects by the Ford Motor Company using engines provided by the Philips Company and the American Motors Corporation (AMC); several cars were equipped with units from Sweden's United Stirling built under a license from Philips. The NASA vehicle test projects were designed by contractors and designated MOD I and MOD II (Nightingale, 1986).

Stirling engines may also hold theoretical promise as aircraft engines, as long as high power density and low cost can be achieved. They are quieter, less polluting, gain efficiency with altitude due to lower ambient temperatures, are more reliable due to fewer components and the absence of an ignition system, produce much less vibration and use safer, less explosive fuels

(Wikipedia, n.d.). However, the Stirling engine often has low power density compared to the commonly used Otto engine and Brayton cycle gas turbine. This issue has been a point of contention in automobiles, and this performance characteristic is even more critical in aircraft engines. Robert McConaghy created the first flying beta configured Stirling engine powered aircraft in August 1986. The *beta* engine weighed 360 grams, and produced only 20 watts of power. The engine was attached to the front of a modified Super Malibu radio control glider with a gross takeoff weight of 1 kilogram. The best published test flight lasted only 6 minutes (Iwaszko, 2011).

The Stirling engine could be well suited for underwater power systems where electrical work or mechanical power is required on an intermittent or continuous level. General Motors has done a considerable amount of work on advanced Stirling cycle engines, which include thermal storage for underwater applications. United Stirling, in Malmo, Sweden, is developing an experimental four cylinder engine using hydrogen peroxide as an oxidant in underwater power systems (Wikipedia, n.d.). The Submarine Assistance Great Autonomy (SAGA) submarine became operational in the 1990s and is driven by two Stirling engines supplied with diesel fuel and liquid oxygen. This system also has potential for surface-ship propulsion, as the engine's size is less of a concern, and placing the radiator section in seawater rather than open air (as with land-based engines) allows for a smaller sized engine (Manikeri, 2013). Furthermore, Swedish shipbuilder Kockums has built eight successful Stirling-powered submarines since the late 1980s. They carry compressed oxygen to allow fuel combustion submerged, providing heat for the Stirling engine. They are currently used on submarines of the Gotland and Sodermanlan classes. They are the first submarines in the world to feature Stirling air-independent propulsion (AIP), which extends their underwater endurance from a few days to several weeks; this

capability has previously only been available with nuclear-powered submarines.

In the United States, Stirling Energy Systems (SES) is a systems integration and project management company that is developing equipment for utility-scale renewable energy power plants and distributed electric generating systems. SES is positioned to become a premier worldwide renewable energy technology company to meet the global demand for renewable electric generating technologies through the commercialization of its own Stirling cycle engine technology for solar and other electricity-generating applications. In 1996, SES acquired the patent, tooling, and equipment rights to the world's most efficient solar dish concentrator system – the Dish Stirling. Initially developed in the 1980s by McDonnell Douglas, the Dish Stirling system, as shown in Figure 6, was field-tested by Southern California Edison and Georgia Power for over 175,000 hours between 1982 and 1988 (Wyld Group, 2008). Edison's test data indicated the Dish Stirling out-performed all other solar-to-electric generating systems by a factor of two, yet had comparable start-up costs. SES optimized the McDonnell Douglas dish to operate with a 25 kW Stirling power conversion unit (PCU) developed in Sweden by United Stirling, Kockums and Volvo. SES is in the forefront of developing alternative solar energy and is currently testing its prototype solar dish field in New Mexico. Each dish has two major components, the solar concentrator and the PCU. The 25 kilowatt SES Dish Stirling system has an operating track record of more than 17 years. Since 1984, it has held the world record for efficiency in converting solar energy into grid quality electricity. The solar concentrator is a large parabolic dish lined with 89 mirror facets, as illustrated in Figure 6 below (Sier, 2013).

Figure 6 SES solar dish Stirling system (Sier, 2013)

The mirrors are precisely aligned to concentrate the suns solar energy to the PCU. The dish is equipped with two motors, which allow the dish to swivel and rotate to follow the suns trajectory across the sky throughout the day. The system begins at sunrise, automatically aligning itself with the sun and follows it until sunset when the system enters "night-stow" with the engine at ground level. The dish's PCU, a Stirling engine, consists of four sealed cylinder assemblies with coolers, regenerators and heater heads. The cylinder assemblies consist of pistons, piston rods, and connecting rods domes. The solar energy concentrated from the mirrors fuels the Stirling engine containing hydrogen gas. The engine cycles at a steady rate of 1,800 rpm running an electric generator producing an output voltage of 480 volts at 60 hertz. In a utility-scale plant, the Stirling units are connected to a substation where the power is conditioned and subsequently transferred across the power grid. SES predicts the dish solar Stirling systems to most likely be marketed outside of the United States to countries with strong government commitments to alternative energy sources.

2.2 The Engine

The Green Stirling Engine Power Plant MQP was started in the fall of 2013 by a different team (Chen et al., 2014). Their work on the engine portion of the design is described in this section. The previous team purchased a Chrysler RV2 air compressor to modify into a Stirling Engine. The RV2 unit was originally used in the late 1960's and 1970's as Chrysler's factory air conditioning compressor. The previous team devised a design based on a custom built Stirling engine found online. The custom build used an RV2 unit and a propane burner as a heat source. The project goal was to replicate the custom build and adapt the engine for a green energy heat source.

The first challenge the previous team faced was adaptation of this V-block air compressor into the engine. The previous team removed the caps covering both of the pistons in order to investigate how the compressor could be converted into a Stirling engine. The previous team concluded that one cap could be used as part of the cooler. The heater would need to be completely rebuilt in order to achieve the required material properties. The oil inside the compressor was replaced with 5W-50 motor oil. The 5W-50 oil reduced the friction inside the pistons and on the crankshaft. The Chrysler RV2 had interconnecting chambers not normally present on a Stirling engine. The interconnecting chambers of the compressor were used to place thermocouples throughout the system. Four thermocouples were placed such that they could be used to measure the temperatures at the tops of both the hot and cold pistons, and inside the regenerator.

The hot cylinder head was designed to meet several requirements. First was the ability to transfer heat through the piston head to the expansion cylinder without significant losses. The hot cylinder head must be able to maintain a closed seal on the working fluid system. The previous

team had chosen to base their engine off a dual piston V-block. Cast iron is the piston chamber wall material. Cast iron has low thermal conductivity. Low thermal conductivity results in poor heat transfer into the expansion cylinder. The previous team designed a hot cylinder head with a higher thermal conductivity. The general shape of the heater was a basic rectangular base instead of the original compressor head shape. This change reduced the volume of the part significantly. Aluminum alloy 6061 was selected for the heat transfer plate. This plate design required an alteration of the position of the hole for the mass transfer tube. The diameter of the tube was 1.125 inches. The previous team positioned the hole so that the tube exited normally from the heat transfer plate and then angled 90 degrees away. Aluminum foil was used as sealant between the heat transfer plate and the cap, and around the tubing entering the heater.

The intent of a regenerator in a Stirling engine is to recover as much heat as possible from the air coming out of the expansion cylinder. The design of the previous team's regenerator focused on maximizing the surface area. The final iteration of the regenerator was a copper coil. This was settled on due to ease of construction and low impedance to fluid flow, while maintaining good surface contact area. Copper was chosen as the regenerator material because of its high thermal conductivity. Holes were cut in the thin copper sheet to maximize the exposed surface area. Testing indicated the regenerator was effectively absorbing heat.

The main purpose of the Stirling engine cold side cylinder head is to provide a consistent low temperature to keep the cycle running. In order to meet the design intent of the alpha type Stirling engine, the cold head was designed as an external system. The cold head design was an ice tank that sat on top of the engine cold side cap. The airflow piping comes from the bottom of the cold head and exits through a sidewall. The cold head tank was made out of a sheet of stainless steel and welded into a tank shape. A hole was cut into the bottom center and one hole

cut on the sidewall to fit the airflow piping and elbows. Silicone gasket sealant was then placed between the copper pipes and the tank to eliminate leaks and secure the pipes in position. A rubber mat was stretched over the tank and secured with Velcro tape. The rubber cover was for preventing heat transfer to the atmosphere.

The flywheel of a Stirling engine stores some of the mechanical energy generated in the power stroke of the cycle, and returns it to the crankshaft when the pistons reach their full extension. The previous team utilized several disks of 6061 aluminum. The disks were bolted together, and another bolt was used to attach the assembly to the output shaft of the engine. The connecting bolt was secured by lock nuts. A small gear was attached to allow for power transmission to the generator. The previous flywheel weight was 1.66 pounds and had a radius of 2.725 inches or 0.227 feet. Tests brought the previous team's flywheel to a maximum of 1150 RPM.

In order to test the modifications described above, the previous team needed accurate temperature data. Two type K thermocouples were used, one in the hot piston chamber and one in the hot side of the regenerator. Type K was preferred for this application because of their high temperature resistance. Three type T thermocouples were also used, one directly immersed in the coolant, one in the cold side of the regenerator, and one in the cold piston chamber. The thermocouples were threaded through the vestigial air outlet in the compressor. Unnecessary holes and spaces were sealed with expanding foam and JB Weld to reduce internal dead volume (Chen et al., 2014).

2.3 Green Power

The team considered several waste heat sources as alternatives to solar power. Solar energy offered the highest temperatures. The Stirling engine works directly from a temperature

differential. Solar energy is a readily available source. If solar collection could be proven to gather sufficient energy to theoretically turn the engine, the engine would be able to operate off of various other excess heat sources, and have possible co-generation applications. Also, solar is a major source of renewable, sustainable energy that is accessible as long as the sun is shining. So, the team turned a portion of their efforts to try and successfully harness and focus the energy of the sun in order to prove its viability as a source of energy for the engine.

2.3.1 Solar Conditions in Worcester

To ascertain the effectiveness of the parabolic dish, the team needed to determine the amount of available solar energy present at the time of testing. The best measurement of solar energy for the purposes of the project is Direct Normal Irradiance (DNI). DNI is "the amount of solar radiation received per unit area by a surface that is always held perpendicular to the rays that come in a straight line from the direction of the sun at its current position in the sky" (Vaisala). Data for the monthly average DNI in the Worcester area was available from the National Renewable Energy Laboratory (Cornwall, et al., 2014).

In comparing maximum and average solar energy of Worcester between November, the lowest month of solar radiation, and July, the highest month, there is a ratio of 1.73. This means that a sunny day in July will receive 173% as much $kW*h/m^2/day$ as a sunny day in November. Differences in monthly DNI were kept in mind when extrapolating the results of collected data in low-DNI months to their optimal values in comparatively high-DNI months when maximum solar energy can be obtained.

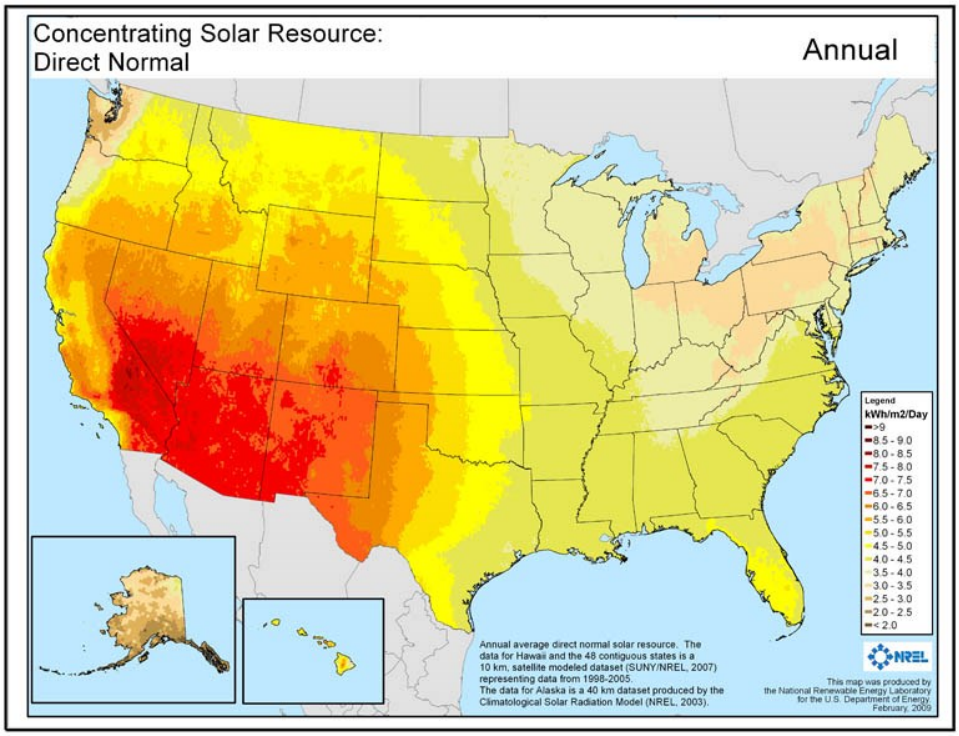

Figure 7 Solar Resource Atlas USA

As seen in Figure 7, Massachusetts is within one of the lowest solar regions whereas the most intense concentrations are in the Mojave Desert, which is a hotbed for solar activity. Using an atlas such as this, it is possible to estimate what our solar capabilities would be if applied in an area of greater solar activity and where solar devices would be most effective.

Annual Average DNI	3.81
January	3.39
February	3.67
March	4.06
April	4.09
May	4.12
June	4.31
July	4.57
August	4.31
September	4.25
October	3.38
November	2.64
December	2.89

Table 1 Worcester Annual Average DNI

2.3.2 Fresnel Lens

The Fresnel lens is formed of concentric lens rings that take parallel rays of light and focus them towards a single point. The modern version used by the previous team is a very thin sheet with the rings so close together that they are indistinguishable and the entire lens resembles a translucent plastic. Other than using it to understand its function and capability, it was not employed in creating further data. The parabolic dish was chosen over the Fresnel lens since the collection area of the Fresnel lens is smaller than the desired collection area. The fabrication of a parabolic mirror proved to be more cost effective than purchasing a Fresnel lens with a larger collection area. The parabolic mirror is also more effective at focusing solar radiation to the focal point than a Fresnel lens of the same collection area (Lorenzo, 1982).

2.3.3 Parabolic Solar Collector

The team decided to pursue a parabolic solar collector instead of a Fresnel lens. Research of modern Stirling engines revealed greater potential energy from a parabolic dish design. The size of a Fresnel lens is limited by manufacturing capabilities. A parabolic dish typically uses a myriad of smaller reflective pieces instead of one large focusing lens. This drives down manufacturing and repair costs. Different reflective material choices can be made for a parabolic dish. The Fresnel lens does not allow the same material choices. Material choice can either increase or decrease cost of the dish. Examples of both are detailed in the following sections.

As explained in section 2.1.3, the team wanted to design a parabolic dish setup modeled after modern installations. Large arrays output greater power, but are expensive. Examples of modern installations can be seen in Figure 8.

Figure 8 Infinia Stirling Engine Solar Array ("30kW Maintenance Free Stirling Engine for High Performance Dish Concentrating Solar Power, 2010)

A small market exists for small-scale Stirling engines. Figure 9 is an example of a small scale Stirling engine powered by a parabolic solar collector. The GT03 dish has a low power output and costs approximately $500. The high cost is driven from precision machined parts and specialty materials. The team therefore sought to design a more powerful low cost parabolic dish.

Figure 9 GT03 (Unassembled Set of Parts) and Solar-Set "Sunshine" ("Stirling Engine Applications,")

Research into low cost solar power arrays revealed a Youtube channel titled "GreenPowerScience". Among many other solar power design projects and ideas, the team found a video containing detailed instructions for building a square solar reflector from cheap materials. The design called for simple low cost materials: wood, a Mylar sheet, strapping tape, caulking, screws, and a half inch pipe section. The video claimed cost could be as low as $25.

Chapter 3: Methodology

3.1 Analyze Need for Engine Improvements

Given the condition of the engine at the start of the project, several modifications were performed to sustain the engine's Stirling cycle. Part of the work was based on the suggestions of last year's team including: theoretical design of a new regenerator, reducing overall dead volume, pressurizing the working fluid, and reducing internal friction. Other improvements to the engine include the design of the flywheel and cylinder heads.

Table 2 Regenerator Calculations

Inner Diameter of Regenerator Pipe (inches)	Volume of Regenerator (cubic cm)	Percent of Engine Volume (cubic cm)	% Mass Transfer
0.125	4.83	5%	95%
0.25	19.32	21%	79%
0.375	43.47	48%	52%
0.5	77.28	85%	15%
0.625	120.75	133%	-33%
0.75	173.89	192%	-92%
0.875	236.68	261%	-161%
1	309.13	341%	-241%

Implementation of a regenerator was considered. Table 2 shows the relationship between tube diameter and mass transfer. In this context, the term mass transfer refers to the displacement of working fluid between cylinders. Increasing the pipe diameter decreases the mass transfer; thus, a smaller pipe diameter is needed to increase the mass transfer between cylinders. Two

options were considered: a 1/8th-inch pipe without a regenerator and a 3/8th-inch pipe with a regenerator. The larger pipe size needed for the regenerator decreases the mass transfer due to the pipe's own internal volume. This, however, is partially compensated for by the volume of the regenerator. Taking into account the surface area of material in the regenerator, the amount of stored energy in the regenerator was calculated and a graph was made that plots surface area vs. energy (in joules) stored.

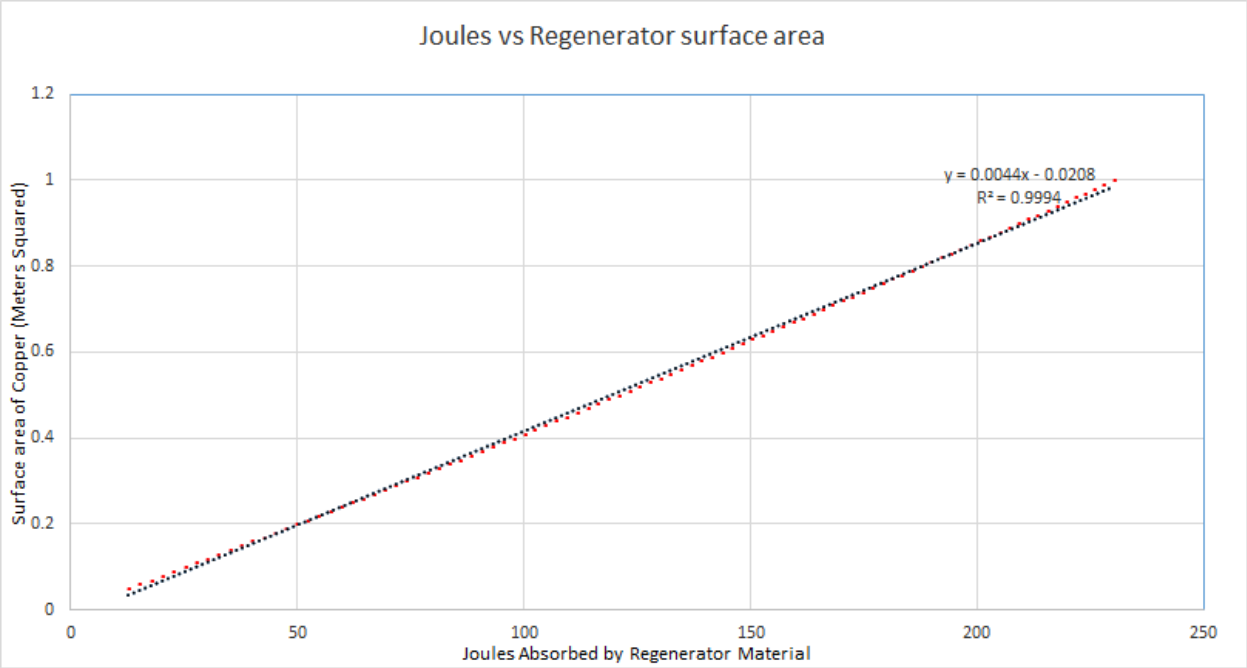

Figure 10 Joules vs. Regenerator Surface Area

3.1.1 Flywheel

Sizing a flywheel requires knowledge of the torque on the object to which the flywheel is attached as a function of crank angle. To accomplish this, the engine's regenerator and each

cylinder were assumed to be isothermal during operation. This allows the calculation of an average temperature by weighting the temperature of each section of the engine by the mass of working fluid in that section. The ideal gas law and existing knowledge of the engine's volumes as a function of crank angle can then be used to find the pressure of the working gas, assuming uniform density. The Mach number has previously been shown to be low, validating the use of an incompressible analysis and the technique proposed.

Working fluid pressure now known as a function of crank angle, the torque exerted on the crankshaft by the working fluid can be determined as a function of crank angle. After the inertial torques have also been accounted for, the total crankshaft torque can then be integrated between the minimum and maximum instantaneous angular velocities to find the energy that the flywheel will need to absorb. The flywheel can then be sized to limit the angular velocity variation to an acceptable range from the needed energy absorption. The process is detailed below.

The working fluid mass can be determined using the initial temperature and pressure and assuming the engine is at maximum volume when initially pressurized using the equation:

$$m_{total} = \frac{P_i}{RT_{i_i}} V_{max}$$

And the average temperature can be found using a weighted average

$$T_{ave} = \frac{V_{hot}T_{hot} + V_{regen}T_{regen} + V_{cold}T_{cold}}{V_{total}}$$

The pressure can be found as a function of crankshaft angle, with the volume already known as a function of crankshaft angle with the ideal gas law in the form:

$$P = \frac{V_{total}}{m_{total}} RT_{ave}$$

The gas force is the difference between the pressure on the two sides of the piston times the area of the piston. The pressure on the backside of the piston is assumed to be equal to the charge pressure.

$$F_{gas} = (P - P_{intitial}) \cdot \pi \frac{bore^2}{4}$$

And the gas torque on the crankshaft is as follows (the inertial effects of the linkage members will be superimposed later in the calculation). $\Theta_{3\ hot}$ is the angle between the crankshaft and the connecting rod for the hot cylinder and $\theta_{3\ cold}$ is the angle between the crankshaft and the connecting rod for the cold cylinder.

$$\tau_{crank\ gas} = r_{crank} F_{gas} \cdot [\sin(\theta_{3\ hot}) + \sin(\theta_{3\ cold})]$$

The inertial toque can be determined using equation 13.15e from *Design of Machinery* (Norton, 2012). In this equation, m_b is the mass at the wristpin in the lumped model of the linkage, r is the eccentricity of the crankshaft and l is the length of the connecting rod. The total torque is then merely the sum of the existing torques.

$$\tau_{crank\ inertial} = \frac{1}{2} m_b r^2 \omega^2 \left(\frac{r}{2l} \sin(\theta) - \sin(2\theta) - \frac{3r}{2l} \sin(3\theta) \right)$$

$$\tau_{crank} = \tau_{crank\ inertial} + \tau_{crank\ gas}$$

The energy that needs to be absorbed can be integrated over the period where the most energy is put into the flywheel without the torque on the crankshaft changing sign. The needed flywheel mass moment of inertia can be found from the needed energy absorption. The coefficient of fluctuation, *k,* is the percentage by which the flywheel speed is allowed to change. For this calculation, it was taken to be 5%.

$$E = \int_{\theta(\omega_{min})}^{\theta(\omega_{max})} \left(\tau_{crank} - \tau_{crank\ avg} \right) d\theta$$

$$I_s = \frac{E}{k \omega_{avg}}$$

The mass moment of inertia for the flywheel designs can then be found in CAD.

3.1.2 The Crank Shaft

To further reduce friction within the engine, the bronze oil lite sleeve bearing that the end of the crank shaft sat in was replaced with a needle bearing. The interface between the crankshaft and sleeve bearing were ample for the as an air compressor, but the friction created was too much for its new application as a Stirling engine. To create enough room for the needle bearing, the diameter of the end of the crank shaft needed to be reduced approximately 140 thousandths. To take the 140 thousandths off, crankshaft was ground using a between centers grinding technique. The live center on the lathe was ground true to the machine and mated with the crankshaft by a centered hole that was drilled into the end of the crankshaft. The dead center on the lathe mated with the threaded hole already present on the crankshaft used to attach the flywheel. Approximately 130 thousandths was taken off initially and then one thousandth at a time was removed until the crankshaft fit well into the needle bearing.

Figure 11 Crankshaft prior to being ground down

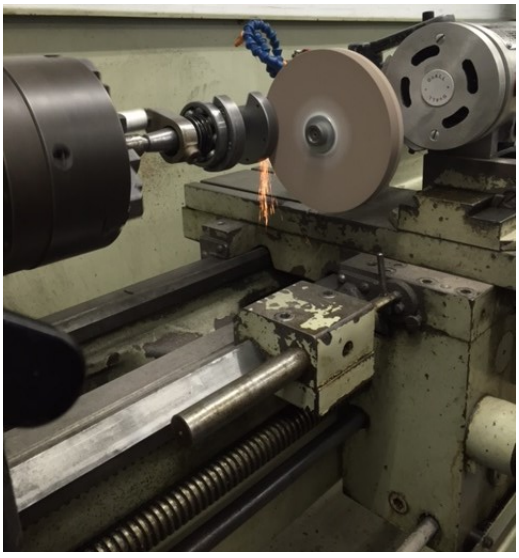

Figure 12 Crankshaft being ground down

3.2 Analyze Need for Energy Transfer Components

Beyond the primary goal of getting the engine to run in the first place, one must also consider what to do with the shaft work being put out. Last year's team purchased a Windzilla 12V DC generator motor, so the current team chose to test its performance and use it to convert shaft power to electrical power. From here, the engine and generator shafts needed to be connected, which led to the design of a transmission, and subsequently, a frame to hold everything together. The transmission was designed as a rudimentary v-belt and pulley system, with an additional idler pulley attached to a belt tensioner. The frame is a simple rectangular prism constructed from square steel tubing with a steel baseplate, to which the various components are bolted. The final piece of the power transmission system is storing or using the electrical power in some way. To accomplish this instead of simply dissipating it as heat, a charge controller, battery, and a large resistor were purchased. The following sections outline the design process for the above described components.

3.2.1 V-belt Transmission

The Stirling engine output shaft and generator shaft were modeled in SolidWorks; these shafts serve as the input and output of the transmission, respectively. The two pulleys were Type a V-belt pulleys with outer diameters of 6 and 2 inches, for the engine and generator, respectively. These sizes are estimates based an assumed natural RPM for the engine and a target RPM for the generator to produce a given amount of power. The target generator RPM was estimated from a power curve graph provided by the manufacturer of the generator, in order to produce approximately 250 W of power. As seen in Figure 13, the generator produces 25 volts

and 10 amps while spinning at 2300 RPM. Power is calculated as the product of voltage and

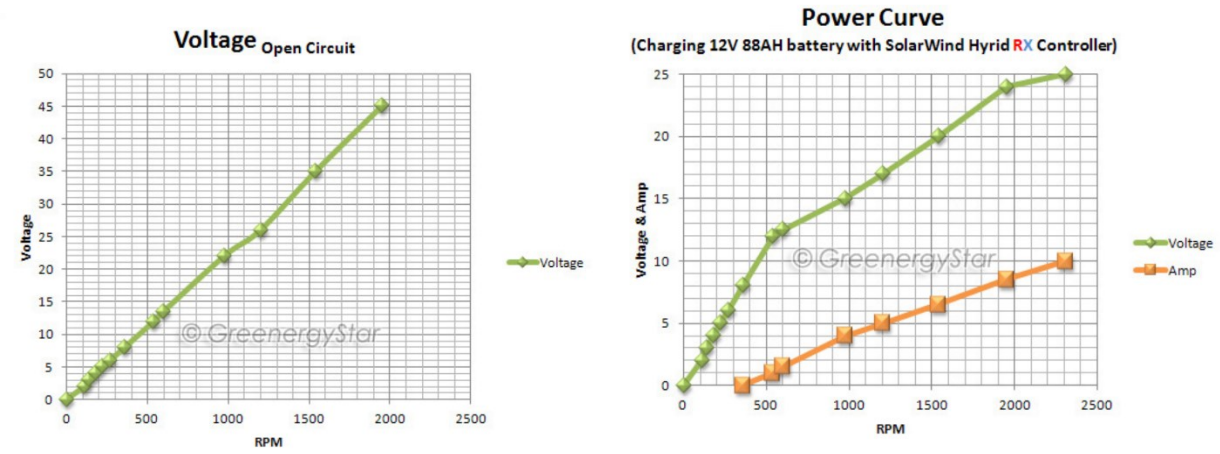

Figure 13 Generator open circuit voltage and power curve (WindZilla 12 V DC Permanent Magnet Motor Generator for Wind Turbine PMA.)

current, yielding the target generator speed.

$$Assumed\ Engine\ RPM = 800\ RPM \quad Target\ Generator\ RPM = 2300\ RPM$$

$$Required\ Pulley\ Size\ Ratio = \frac{2300}{800} = 2.875$$

$$Smallest\ available\ pulley\ diameter = 2" \rightarrow Larger\ pulley\ diameter = 5.75"$$

Since a 5.75 inch pulley was not available for purchase, a 6 inch pulley was selected instead, which would require a lower torque from the engine to drive the generator. Given that nearly all v-belt pulleys have uniform cylindrical bores, and the engine shaft is tapered, it was required for the team to design and build an adapter in order to mount a pulley to the engine.

Additionally, the shaft of the generator is threaded, as well as metric size—which meant that an adapter would be required to connect a traditional US size V-belt pulley to this shaft as well. Figure 14 below shows a SolidWorks model of the shafts and pulleys.

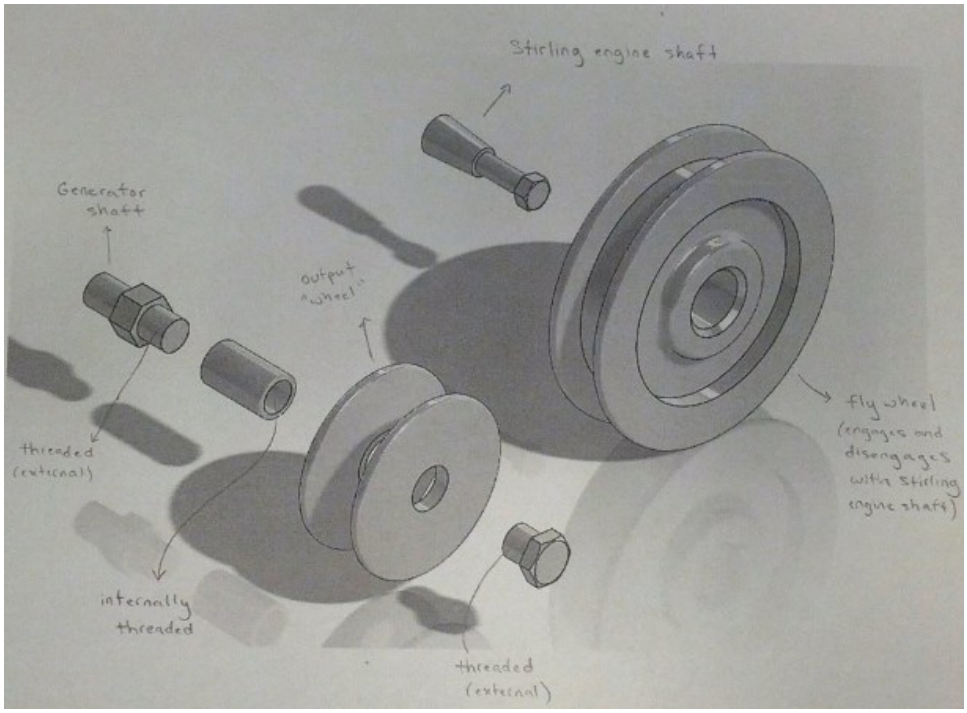

Figure 14 Model of Pulleys and Shaft

In order to attach the engine pulley, a single adapter was machined that mounted onto the tapered shaft using the included set screw, and provided a uniform shaft for the pulley to mount to, as well as a larger shaft with a flange for mounting the flywheel. The design of this part is covered under the flywheel section. Figure 14 above also shows a proposed solution for mounting a pulley to the generator shaft. The concept is to get a metal sleeve that is internally threaded to accept the generator shaft, mount the generator pulley on that sleeve, and cap it off with a hex bolt. However, instead of spending valuable time machining a threaded sleeve, the

team elected to machine a simple, unthreaded sleeve that mates with the generator shaft via transitional fit and mount the pulley on that with a set screw.

With the pulleys securely mounted to their respective shafts, the transmission needs one additional component to minimize slip between the belt and pulleys—a belt tensioner. Tensioners are generally basic assemblies that consist of an arm with an idler pulley attached, which has torque acting on it. Most commercial belt tensioners are made for automotive serpentine belts and tend to be relatively expensive. An exploded view of a serpentine belt tensioner is shown in Figure 16.

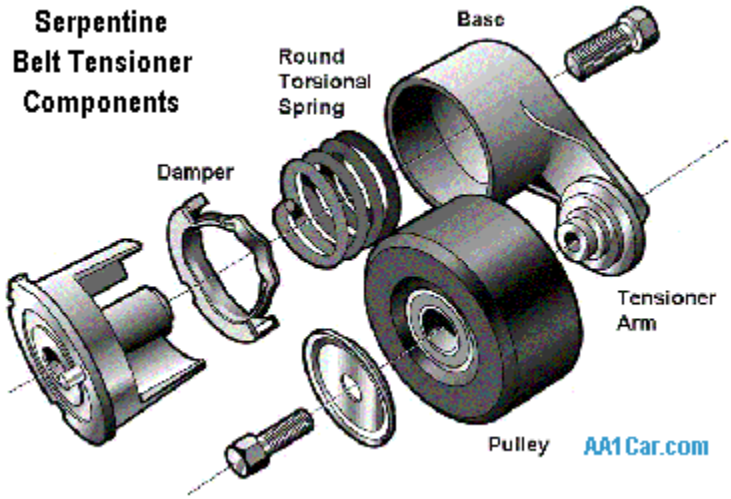

Figure 15 Slot-mounted idler tensioner

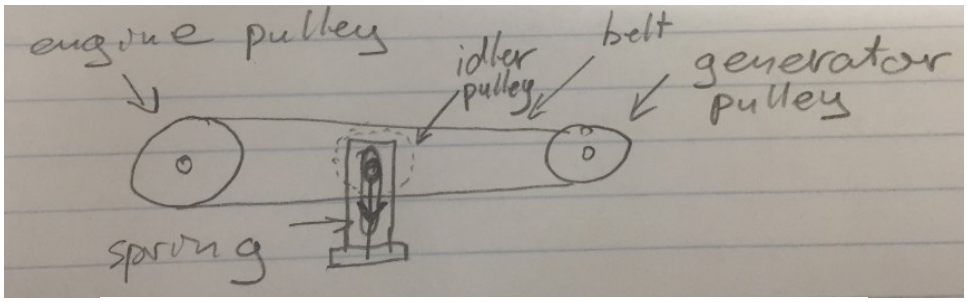

Figure 16 Belt tensioner exploded view (Automatic Belt Tensioner.)

Given these circumstances, the team chose to design a custom belt tensioner in order to save money and have a more suitable product for this project. One potential design was composed of an idler pulley whose shaft would be slot-mounted between two plates. The shaft would be pulled down by springs on both sides in order to tension the belt. A sketch of the idea is shown in Figure 17.

Another potential design was modeled more closely to a traditional serpentine belt tensioner. It is composed of a vertical aluminum plate that is mounted perpendicular to a horizontal plate. The vertical plate is connected to an arm with a spacer and hex bolt to allow the arm to rotate. Both the vertical plate and the arm have a spring anchor connected to them, which would allow the arm to pulled upwards, pushing the pulley against the inside of the V-belt. A SolidWorks model of this design is shown in Figure 18.

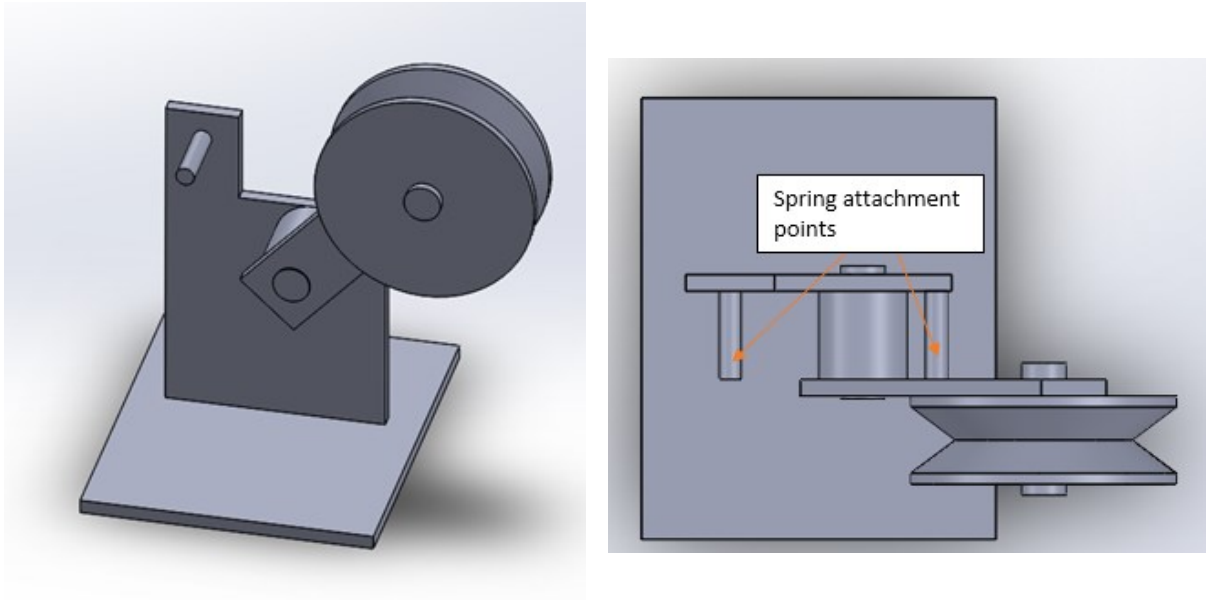

Figure 18 Serpentine-style belt tensioner

The serpentine-style belt tensioner was chosen for further development because it is much more stable than the slot-mounted design and allows for easier access to the belt after

installation. In order to find the proper spring for use with this tensioner, a belt-tensioning guide by Carlisle Power Transmission Products was followed, which provided the following relations (V-Belt Tensioning, n.d.):

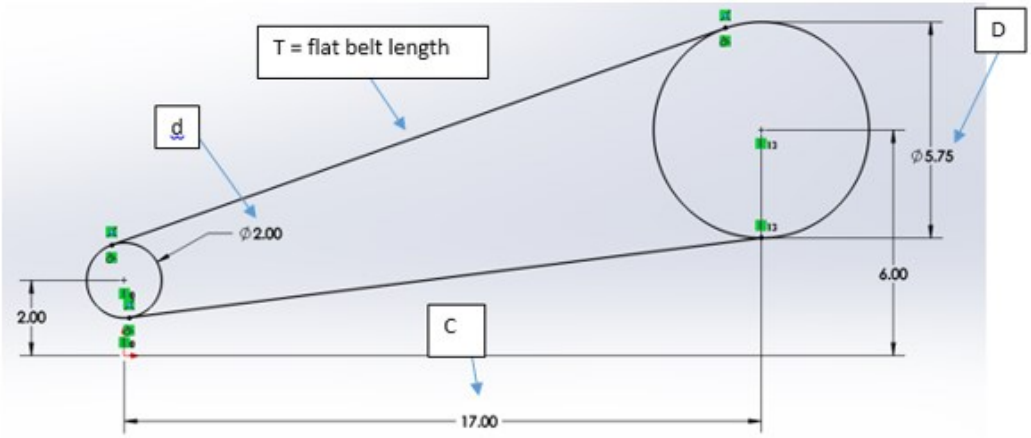

Figure 19 Belt-Tensioning guide relations

$$Flat\ belt\ length = \sqrt{C^2 - \left(\frac{D-d}{2}\right)^2} = \sqrt{17^2 - 2^2} = 16.88\ inches\ [0.429\ meters]$$

$$Strand\ tension = \frac{Horsepower * K}{Q * S}$$

$$Assume\ Horsepower = \frac{1}{3}$$

$$K = constant\ from\ guide = 26.172$$

$$Q = number\ of\ belts = 1$$

$$S = belt\ speed\ in \frac{\frac{ft}{minute}}{1000} = engine\ speed * engine\ pulley\ radius$$

$$800\ RPM * 2\pi \frac{radians}{rotation} = 5026.6 \frac{radians}{minute}$$

$$Engine\ pulley\ diameter = 6\ inches = 0.5\ feet \rightarrow engine\ pulley\ radius = .25\ feet$$

$$S = \frac{5026.6 * .25}{1000} = 1.257 \frac{\frac{ft}{minute}}{1000} \left[0.3831 \frac{\frac{m}{minute}}{1000}\right]$$

$$Strand\ tension = \frac{\left(\frac{1}{3}\right) * 26.172}{1.257} = 6.94\ lb\ [30.87\ N]$$

$$Y = constant\ based\ on\ belt\ type = 6$$

$$Min\ deflection\ force = \frac{strand\ tension + Y}{16} = \frac{6.94 + 6}{16} = 0.809\ lb\ [3.60\ N]$$

$$Max\ deflection\ force = \frac{(strand\ tension * 1.5) + Y}{16} = \frac{(6.94 * 1.5) + 6}{16}$$

$$= 1.026\ lb\ [4.56\ N]$$

For the preliminary design, a belt deflection force of 1 lb was assumed. However, since the spring is not pulling directly on the pulley, the spring force needed to be derived in accordance with the geometry of the tensioner.

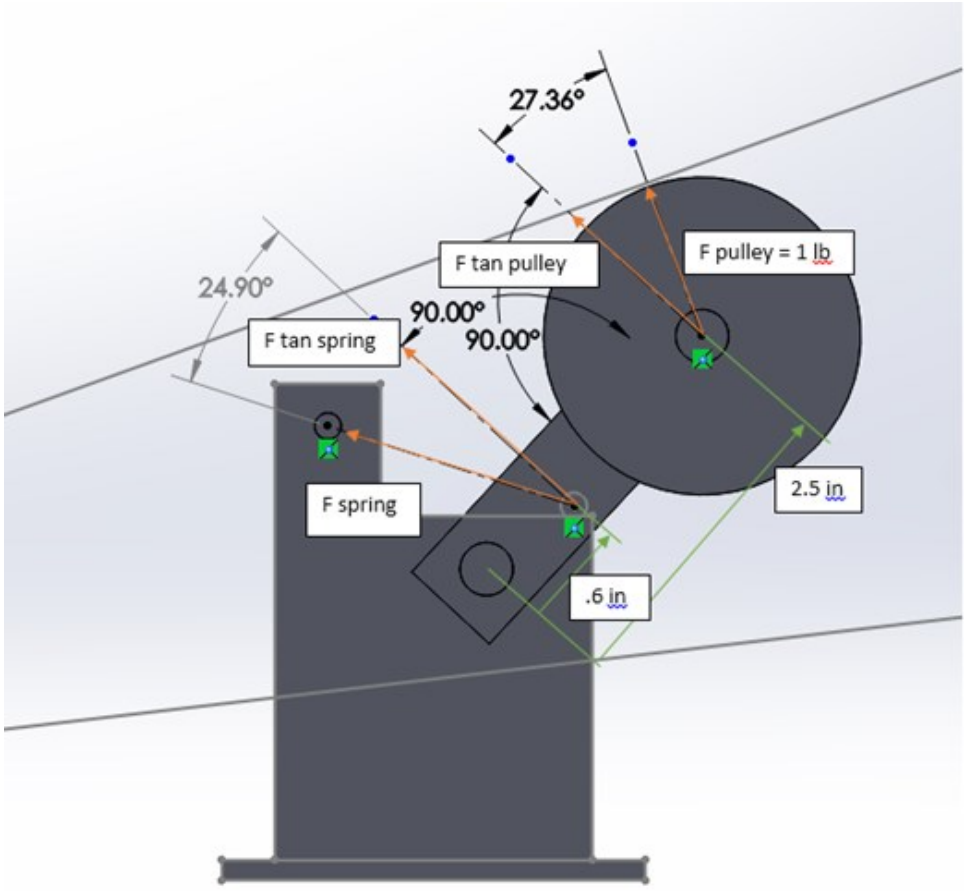

Figure 20 Tensioner Calculations Diagram

$$F_{pulley} = 1lb\ [4.45\ N] = F_{tanpulley} * \cos(27)$$

$$\Rightarrow F_{tanpulley} = 1.12\ lb\ [4.98\ N]$$

$$F_{tanspring} * .6 = F_{tanpulley} * 2.5$$

$$\Rightarrow F_{tanspring} = 4.66\ lb\ [20.73\ N]$$

$$F_{spring} * \cos(25) = F_{tanspring}$$

$$\Rightarrow F_{spring} = 5.14\ lb\ [22.86\ N]$$

After purchasing the materials needed to build the tensioner, the layout of the transmission changed slightly, so the tensioner design was refined to increase clearance between the belt and other components. The most prominent changes include rotating the tensioner on its side so that it pulls down on the belt instead of pushing up, as well as moving the spacer from between the arm and the base, to between the arm and the idler pulley. These changes allow for more stability of the tensioner due to a lower profile, and for less interference with the belt, due to the altered spacer location. The final tensioner design is shown in Figure 21.

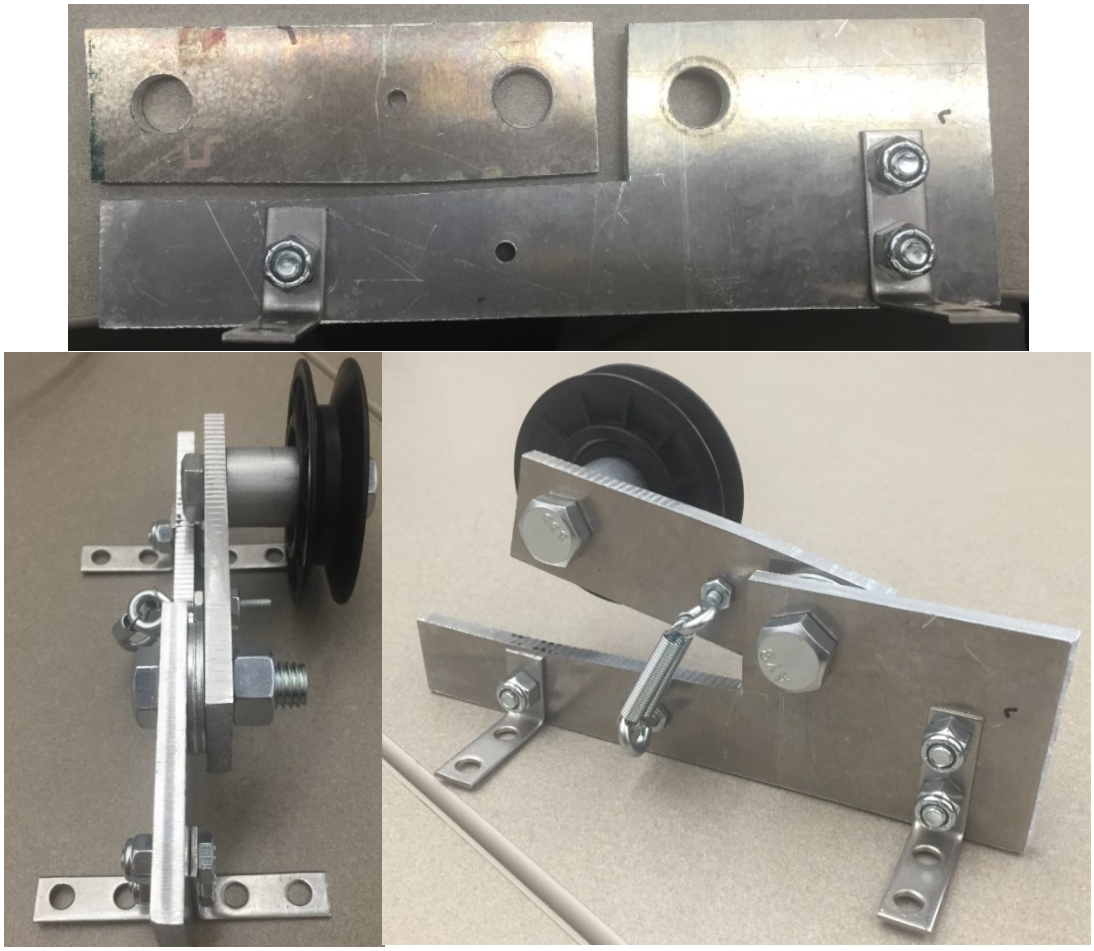

Figure 21 Final Tensioner Assembly

3.2.2 Frame

The purpose of building a frame is to safely consolidate the engine-related components of this project on a sturdy base, as well as to reliably line up the different sections of the V-belt transmission. Initially, commercially available engine mounts and frames were considered, however, none of the products reviewed met the size requirements and price constraints of the project. Instead, a custom frame was designed in SolidWorks.

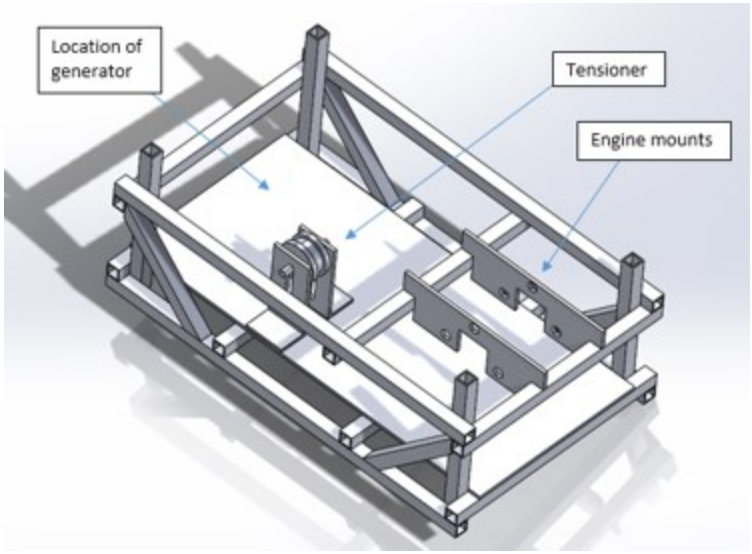

Figure 22 Frame Iteration 1

The frame was designed to accommodate the following: the Stirling engine, the generator, and the tensioner. Figure 22 shows the earliest iteration of the frame design. This version requires too much material, and involves cutting and drilling at 45 degree angles. Additionally, joining the square tubing in this design would involve drilling a large number of holes, which would look unprofessional and weaken the material. This design was simplified and refined to yield the next iteration, shown in Figure 23.

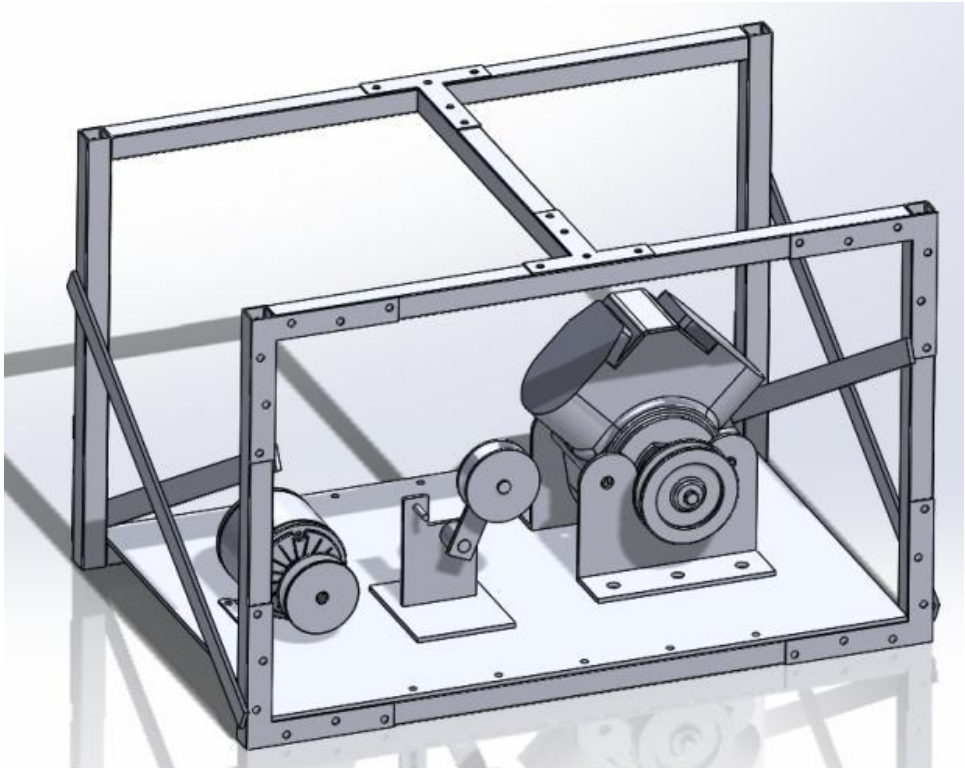

Figure 23 Frame Iteration 2

The changes made to Iteration 1 are the addition of brackets to hold the tubing together instead of bolts alone and the omission of 45° cuts and unnecessary strengthening components. Furthermore, the frame is taller, and the engine is mounted to the baseplate, as opposed to hanging down from the top of the frame. This design was chosen for final production.

Several different materials were considered for building this frame based primarily on cost and aesthetics. The major candidates were square steel tube stock, 90 degree angle steel stock, perforated 90 degree angle steel stock, and rectangular aluminum tubing. While the 90 degree angle stock options were the cheapest, the square steel tubing would look more professional, so it was chosen as the primary material for the frame. The material for the baseplate was chosen as 14 gauge steel sheet because of its strength, formability and relative low cost.

The square tubing was cut using a band saw, de-burred, and drilled with the proper holes for assembly. The frame joints were sandwiched between two brackets and held together with machine screws and lock nuts. With all the corner brackets installed, the frame was strong enough to omit the cross-braces from the design in Figure 22. Assembly of the frame is shown in Figure 24.

Figure 24 Assembly of the Frame

A plasma cutter was chosen to roughly cut the baseplate to size, and a disk grinder was used to make straight edges and clean up the material. After the baseplate was cut, holes were drilled through the baseplate and frame in six locations in order to join the two using machine screws. The final product is shown in Figure 25.

Figure 25 Frame and Base Plate

3.2.3 Engine Mount

The interface between the engine and frame was designed to affix the engine to the frame securely and as close to vertically as possible, and leave enough room for the flywheel to spin freely. Consequently, the engine mount was designed around the dimensions of the flywheel. It is comprised of four steel plates cut from the same material as the frame baseplate. Two plates with flanges are located on either side of the engine. Two additional plates connect to the flanges in order to make a box-like structure. The engine is mounted between the first two plates using two large bolts. A model of the design is shown in Figure 26:

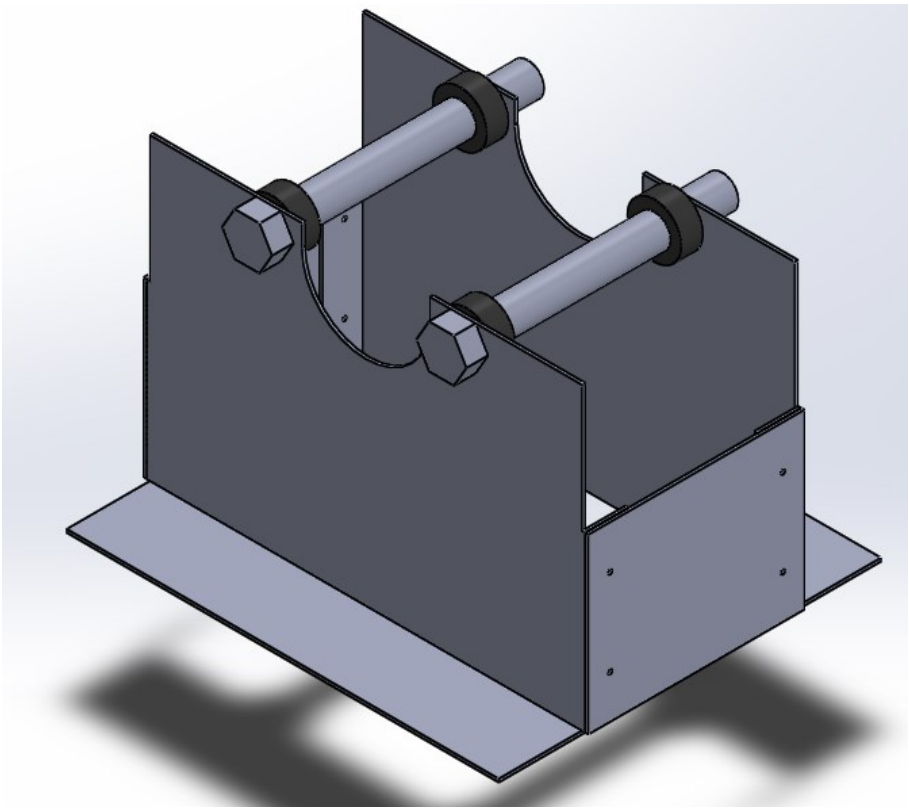

Figure 26 CAD model of Engine Mount

The vertical flanges which join with the sides of the mount are connected by ¼ inch bolts with lock nuts. The horizontal flanges have holes drilled through them, in order to interface directly with the baseplate of the frame. A plasma cutter was used to make the rough cuts in the material; the flanges were cut out with a hacksaw, cleaned up with a disk grinder, and bent with a brake. Pictures of the process are shown in Figure 27:

Figure 27 Engine Mount Fabrication

The U-shaped profile was cut with the plasma cutter and grinder to allow the engine shaft to protrude, while the bolt holes were drilled. An angle grinder was used to round the corners of the engine mount for added safety and aesthetics. Figure 28 shows the engine mount in use with the engine and the flywheel attached.

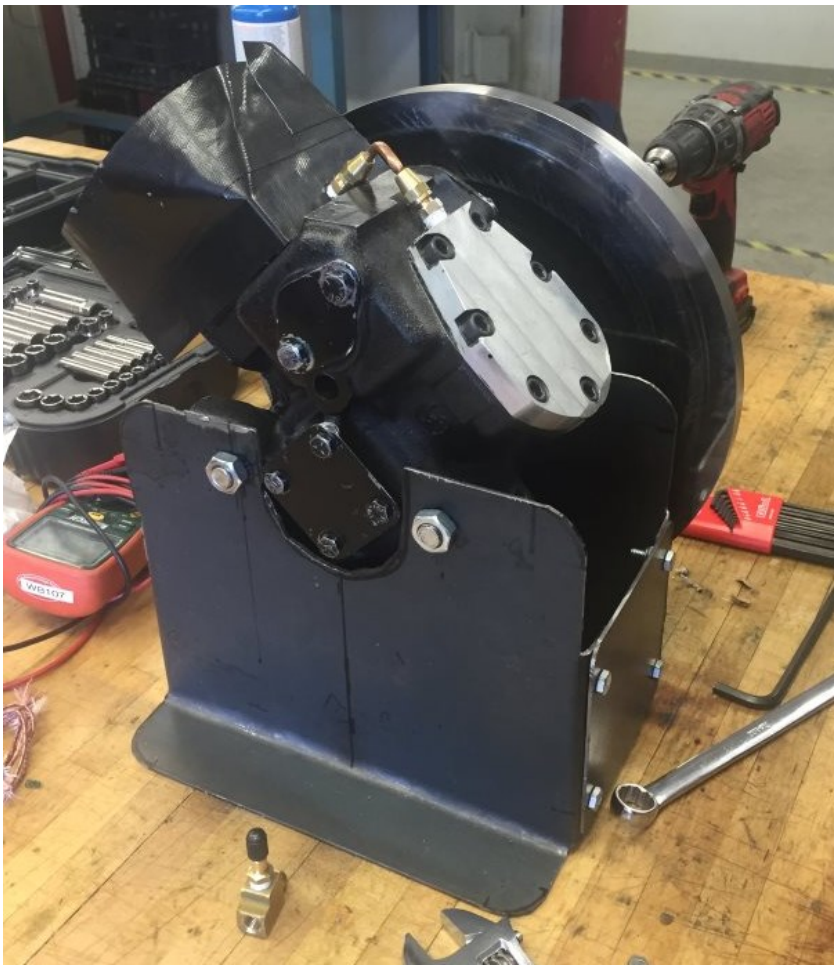

Figure 28 Engine with Mount

3.2.4 Generator Mount

Instead of bolting the generator directly to the baseplate of the frame, a generator mount was with two axes of adjustability to compensate for potential changes in pulley sizes as well as belt stretching was desired. The following adjustable motor mount was purchased from MSC.

Figure 30 Purchased Generator Mount

This mount is only adjustable in one axis through the use of a vise screw, so an additional mounting plate was machined to help interface between the generator and the motor mount. This plate attaches to the motor mount and contains two slots that are perperpendicular to the direction of adjustability of the motor mount. This allows the generator an additional degree of adjustability to ensure proper alignment of the belt transmission system. A SolidWorks model of this adapter

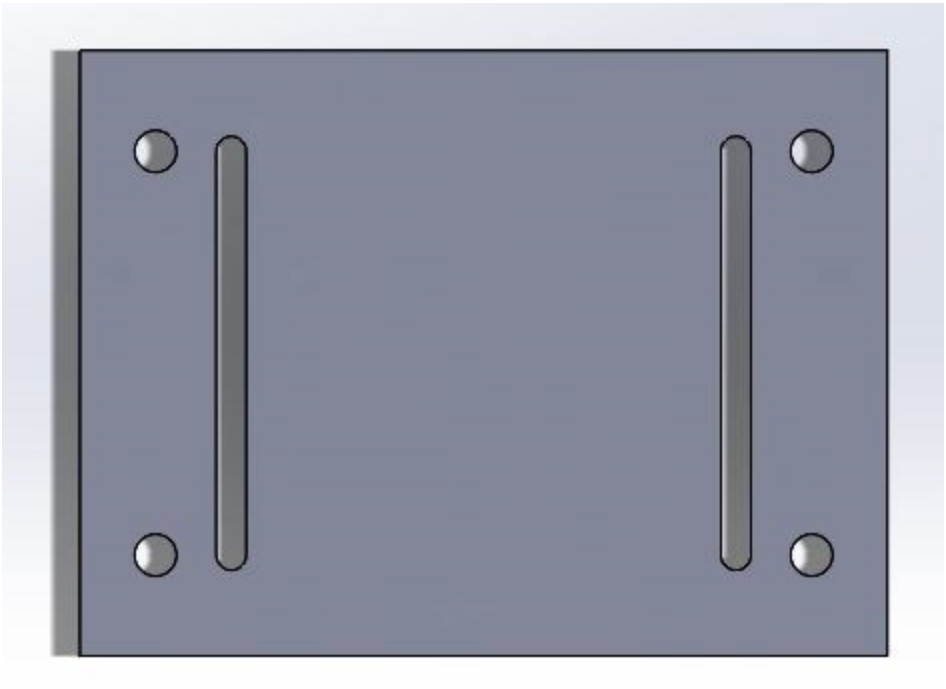

Figure 29 Generator Adaptor Plate

plate is shown in Figure 29.

3.2.5 Electrical Components

In order to store energy produced by the Stirling engine, a battery-charging system was configured. In the final arrangement of the project, the engine turns the generator with a belt transmission, which puts out electrical power. This electrical power is regulated and monitored by a charge controller, and is used to charge a battery.

The chosen charge controller is the Xantrex C35. It was selected due to its low cost, high current rating, and versatile function. It can be used to control charging patterns of a battery, to control the usage of battery power by external loads, or to divert excess power to an external load—which is the most relevant function for this project. The main function of the charge controller is to regulate battery charging in a three-phase protocol. In the bulk phase, the voltage entering the battery is held at a constant value, and the current is kept as high as possible until the battery voltage reaches the bulk setting. In the absorption stage, the voltage stays at the bulk setting while current is gradually reduced until battery capacity is reached. In the final stage, known as the float stage, the source voltage is reduced to a lower user-determined value, and the current is greatly reduced. This mode continues until the battery voltage drops past the float point, at which time a new bulk cycle is initiated. An illustration of the three-phase charging cycle can be seen in Figure 31.

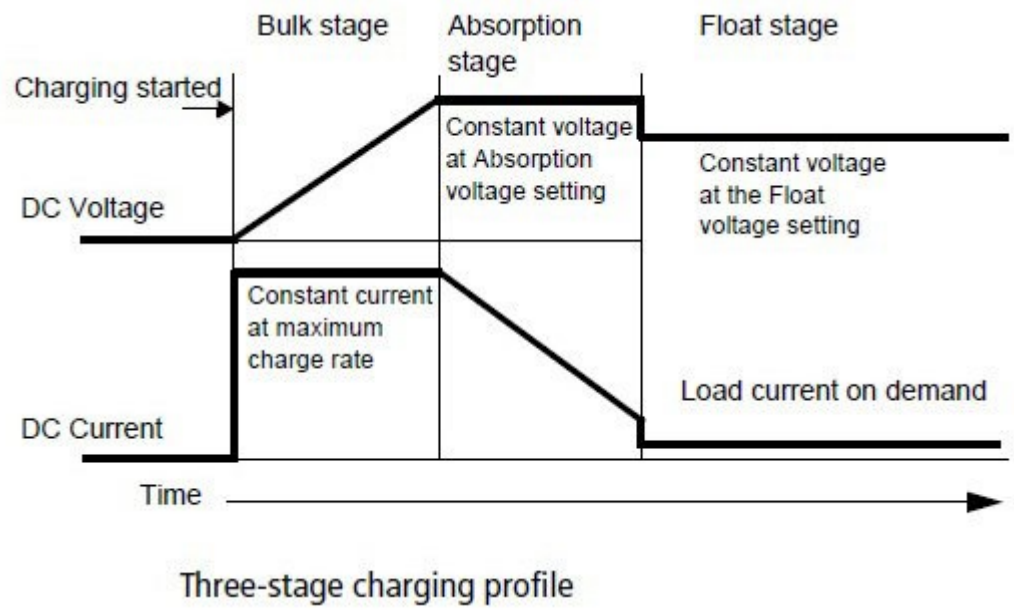

Figure 31 Three-phase charging cycle (C-series Multifunction DC Controller Owner's Manual)

When in diversion load control mode, the charge controller still uses the same three-phase charging protocol, but diverts excess power during each given stage to a dump load. This function protects the battery from overcharging and power surges.

3.3 Solar Collector Design

A parabolic dish was designed and fabricated using wood and Mylar to serve as a solar collector. Several iterations were developed before finalizing the dish design. The operator initially held the dish in place; however, a more precise positioning method was required. The most practical method to accomplish precision was a stand that could pivot the parabolic dish about its elevation axis. The first iteration of the stand was a simple A-frame with a base seen in Figure 1. The A-frame design was decidedly too bulky for practical use. A simpler, more elegant design was proposed as an alternative. The alternative design, shown in Figure 2 utilized a rear-mounted strut to prop the dish at the desired angle.

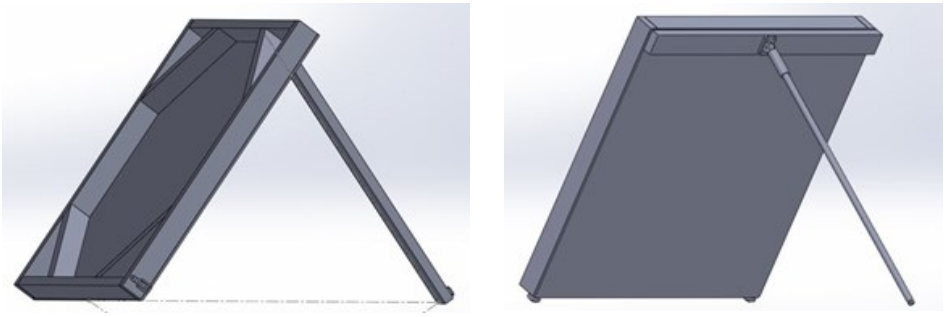

Figure 33 Easel design and pole design (left to right)

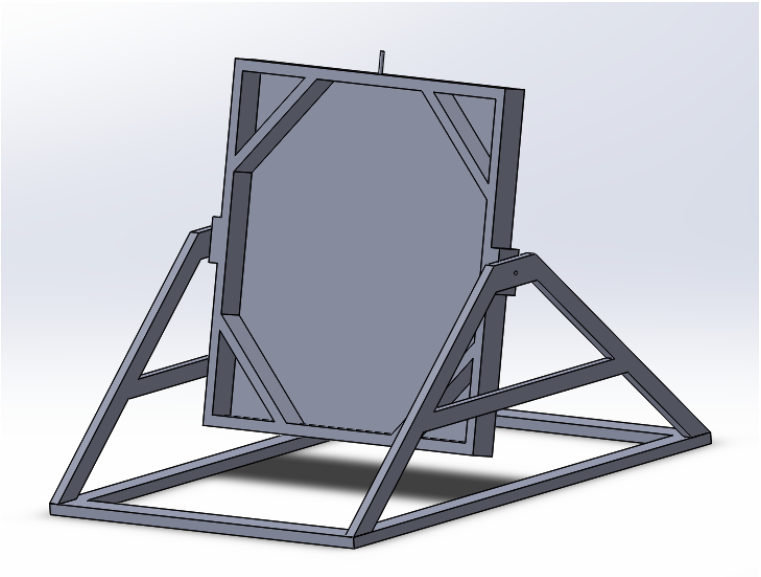

Figure 32 Reflector Dish with A-frame and Square Base

The team advanced the design of the dish by proposing a turntable mount to control the azimuthal adjustment. Four stationary legs would serve as the base mounted on the bottom half of the turntable. This iteration shown in Figure 3 allowed the dish two degrees of freedom and was more compact. Early design iterations included folding legs beneath a stationary sheave disk that supported a Lazy Susan turntable. The mount could swivel atop the turntable with a small motor-driven sheave by rotation a belt around the two sheaves. The problems with this design were the possibility of wobble that a 12 inch turntable would have encountered when trying to

rotate the large mount and the complications in keeping the belt in tension between the two sheaves.

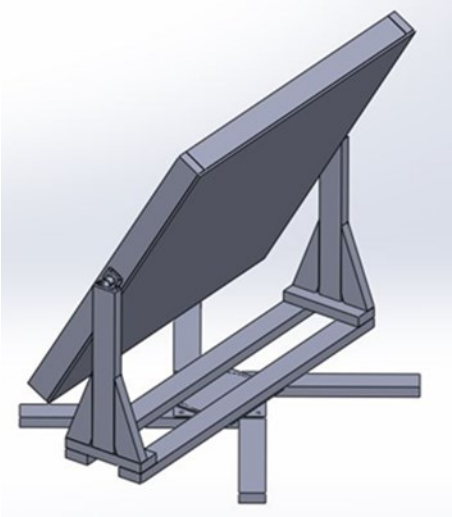

Figure 35 Reflector dish with non-collapsible base

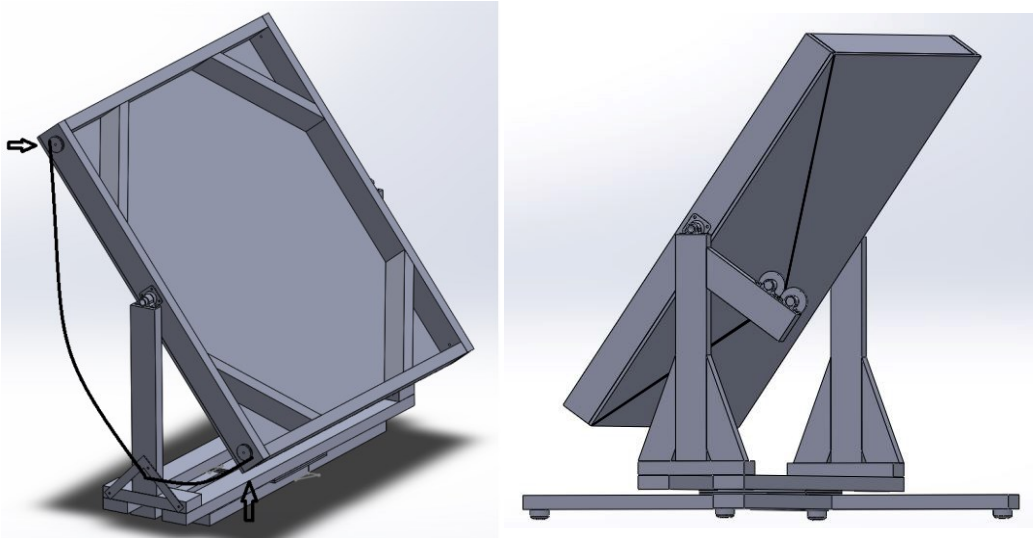

Figure 36 reflector dish and base with proposed pulley system

The team decided under advisement to develop a collapsible base for the reflector dish. Proposed collapsible designs are shown in Figure 37. Essentially, the legs would fold in and out under the rectangular base. Method of elevation adjustment was also reconsidered as shown in Figure 34. A pulley system was developed to provide better adjustment control. A cable hooks to the points that provide the largest moment on the dish and passes around a pulley that can be free spinning or electronically controlled.

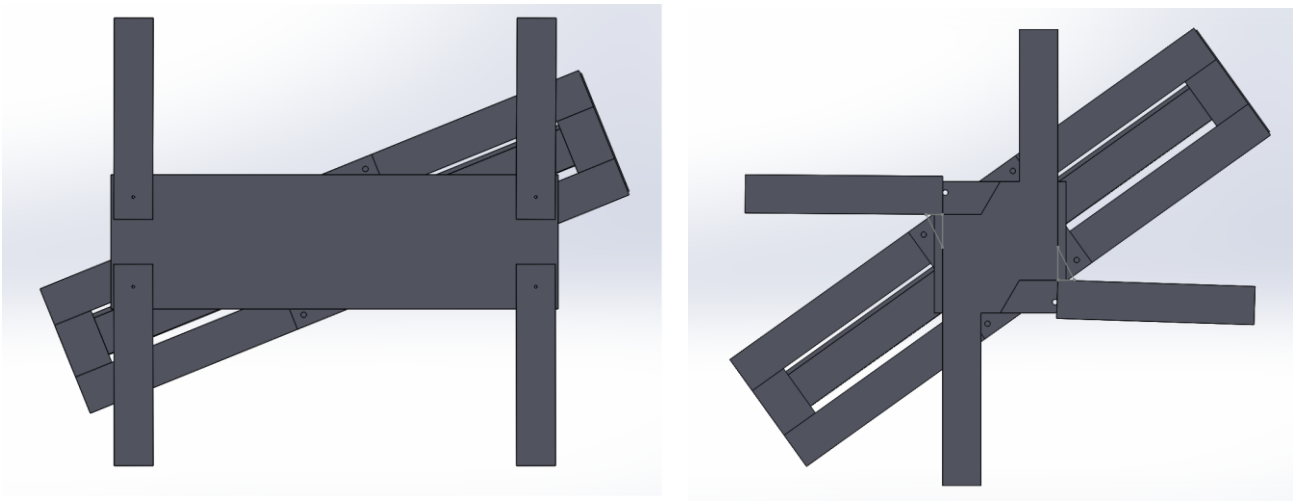

Figure 37 Proposed Collapsible Designs

An alternative to the turntable design was four wheels. Wheels on either end of the base replaced two legs. A perpendicular axle using two independently rotating wheels replaced the other two legs. The axle was intended to be detachable to maintain the collapsibility of the design. Originally, the axle was designed to be triangularly braced to the frame in a fashion similar to Figure 38. The team proceeded in the design process using the wheeled base.

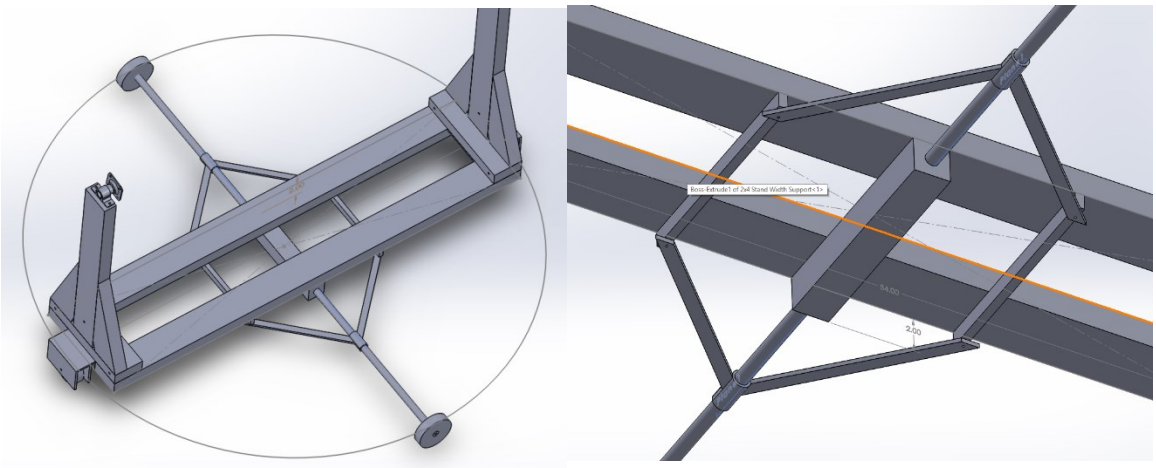

Figure 38 Proposed Collapsible Base with Wheels

For the final design, the angled wood braces were replaced with metal brackets. The triangular braces on the cross axle were removed. The clamps on the axle were determined to produce sufficient strength. The side wheel mounts were replaced by regular castor wheels.

Figure 39 Final Dish Design

The final assembled parabolic dish is shown with a vacuum drawn in Figure 41. The vacuum is drawn from the pipe extending from the top of the dish not shown on the models. The pipe has a ball valve and a cap to retain the vacuum. The cable is an adjustable length bungee cord. The two pulley cable system attached to the rear arm was reduced to one motorized pulley. The cross axle was constructed from copper piping and copper fittings. The copper fittings press fit into the rubber wheels at either end of the axle. The axle is held in place by two clips attached to the bottom of the frame.

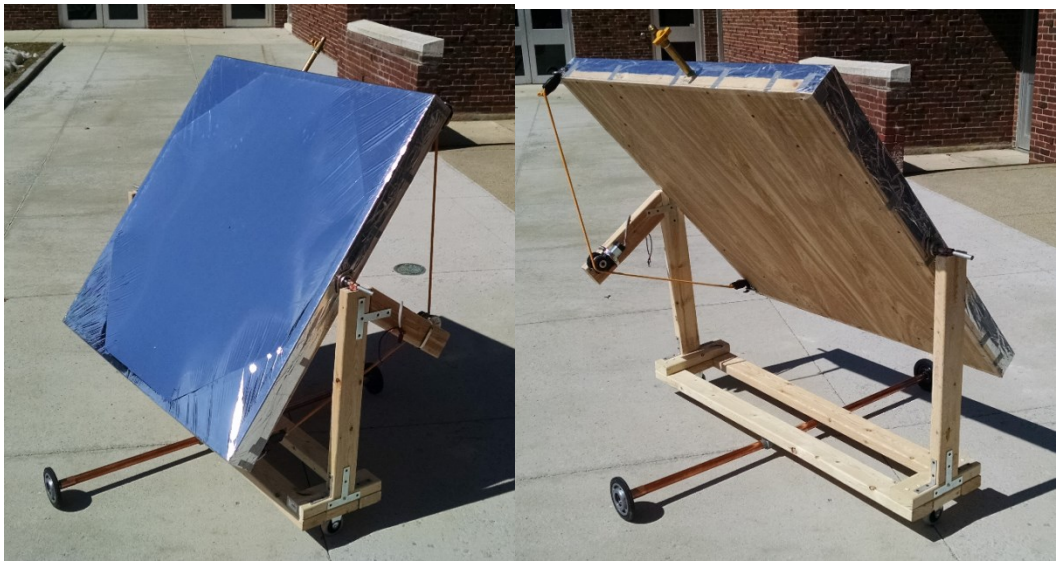

Figure 41 Assembled Solar Dish Front and Back

Figure 40 Assembled Dish Side Views

3.4 Solar Power Data Collection Process

The process for collecting data from the reflector dish is detailed in the following sections. Data collection was dependent on weather conditions, time of day, and test materials.

3.4.1 Creating the Parabola

A parabolic mirror has a focal point along its axis of symmetry. Industrial-scale Stirling engines powered by solar energy are mounted on a long boom to be perfectly positioned at the dish's focus (see Figure 6 on page 32). Holding the engine at a fixed distance would not be practical because the slow pressure leak would gradually alter the distance of the focal point.

To power the engine, the focal area would have to be no larger than the area of the engine's hot head. Any larger and the reflected light would not be properly received. According to research and experiments, an off-axis dish creates a focal area instead of a point, with greater off-axial tilt resulting in a larger dispersion. The focal area was found to be roughly three inches in diameter during tests. A three inch diameter focal area is adequate for the engine head.

The valve used on the mirror is rated for 0.5 psi gage, which managed to achieve a steady depression of 1.25 inches, which creates a focal length of roughly 8 feet. There is enough elasticity in the Mylar to reach the bottom of the frame and create a depression of 3.5 inches, which creates a focus point only 3 feet away from the mirror. The fully-evacuated reflector is tight as a drum and the creases in the Mylar are nearly invisible. Based on these observations, the reflectivity was assumed to be its ideal value of 95% for calculation purposes.

3.4.2 Stand and Adjustment

A cable-pulley mechanism was used to control the elevation of the mirror, as this style of mechanism would be subject to a lesser moment than the other proposed designs. In this

arrangement, a cable would be attached to the top and bottom corners of whichever side of the mirror frame was preferred and a pulley would be mounted onto a branch off the vertical mounting arm. This concept was appealing as it was less mechanically complex and did not require components that would not be easily available.

However, a SolidWorks sketch of this system quickly revealed a problem: the necessary cable length throughout the range of elevation motion was not constant. A Mathcad equation (see Figure 72) was created to model the output cable length based on the dish angle and the position of the pulley sheave. Further iterations of the pulley setup were modeled and the optimal configuration involved angling the pulley arm at an angle equal to 90° minus half of the maximum elevation.

The NOAA Solar Position Calculator was used to calculate the maximum solar elevation for Boston, Massachusetts. The average maximum annual elevation occurs at noon on June 21st and was 70.89° above the horizon. The maximum elevation was then set to 70° for calculation purposes. This made the optimal angle pulley angle 55°.

This design incorporates a 12-inch pulley arm and has a rope length difference of 1.5 inches. Increasing the length of the pulley arm lessens the force that must be applied to overcome its moment, but also increases the lengths that the cable must stretch as the dish moves from vertical to nearly horizontal. Figure 42 illustrates the variation in cable length as function of arm length in inches. The elevation angle is held constant at 0° and 35°, which are the two angles in which the changes are most severe, and the delta is then calculated. The first possible solution is that the pulley is kept in tension by a spring. The second is that an elastic cable is used. An elastic cable is a simpler solution that would eliminate the need to construct the entire pulley mount on a spring, though its disadvantages could be that it could be more elastic than is

required in regards to frictional forces. This could allow the dish to move slightly in the wind, which would throw off the focus from the target.

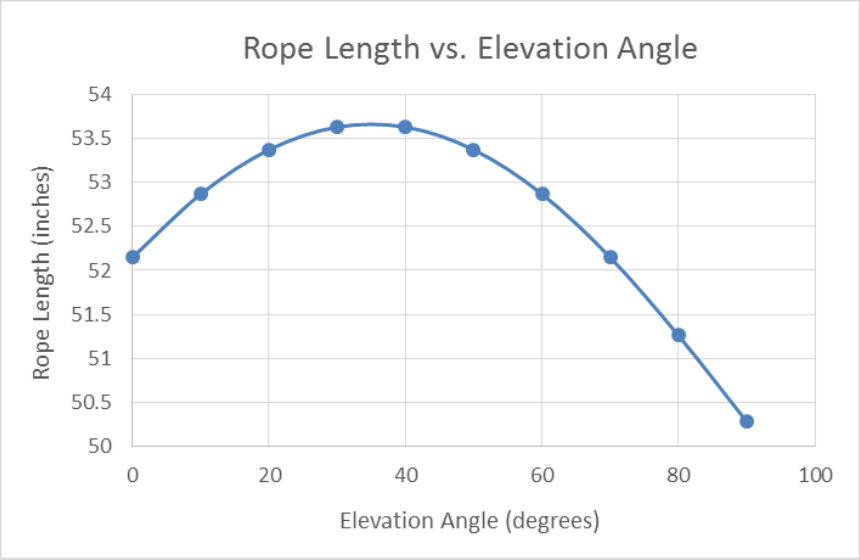

Figure 42 Rope Length vs. Elevation Angle

Early dish mounting iterations included folding legs beneath a stationary sheave disk that supported a 'Lazy Susan' turntable. The early mount design swiveled atop the turntable with a small motor-driven sheave by rotation a belt around the two sheaves. The problems with this design were the possibility of wobble that a 12-inch turntable would have encountered when trying to rotate the large mount.

The iteration chosen as final equipped the frame with wheels at each point of the compass and did away with the turntable, sheaves, and legs to be more weight-efficient, portable, and less mechanically complex. Instead of turning the stand on a pulley, the entire stand turned itself by spinning one or both of the side wheels. For stability, a long central shaft was mounted with its axis perpendicular to the front of the frame served as an extension for two more wheels to be attached. The shaft does not spin and the wheels have built-in bearings that can rotate independently. Detachment was necessary to allow the shaft to be taken off the frame for

transportation purposes. Ergo, the shaft was attached to the mount by compliant ratcheting pipe clamps that allowed for relatively easy detachment without the need for tools.

Stability was analyzed by estimating the wind forces required to tip the frame. The weakest situation would be when the wind is blowing exactly between any of the "legs", which reduced the effective base of the frame from 52" to 37". This reduction was effectively the tipping of a square about its side instead of an axis on its corner that was farther from the center. The tip of the leg would then serve as the zero length and the moment caused by wind could be compared to the moment caused by the weight of the frame. The tipping point comes when the wind moment, as calculated by the drag equation using the dish area, overcomes the weight. The dish was measured to weight exactly 30 pounds, making our mount variants including the dish weigh in the region of 50-60 pounds, which is still a manageable two-person load.

3.4.3 Weather Conditions

To maintain uniformity in testing conditions, testing was reserved for days that were effectively cloudless. A thin layer of clouds significantly impedes direct sunlight. Wind is also a factor to consider in the convection calculations. Similarly, temperature was accounted for using

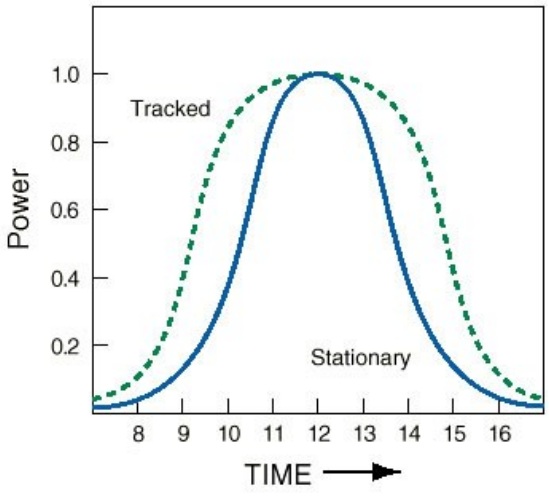

Figure 43 Fractional Power Output for Tracked and Stationary Array

the appropriate heat transfer calculations.

As shown Figure 43, the daily variation in solar energy follows a bell curve. According to the graph, midday is the optimal time to collect solar energy. However, tests were conducted in the early afternoon and Figure 43 was used to extrapolate what results would have been at noon (denoted as 12 on the time axis of Figure 43). The dish was positioned with varying azimuthal while still focusing on target. Therefore, the test results were consistent with the tracked curve in Figure 43.

3.4.4 Initial testing Methodology

All of the early testing was performed manually holding and adjusting the parabolic dish. The test setups are shown in Figure 44. Required items to perform solar testing were a Multimeter, stopwatch, a thermocouple and a target material to receive the reflected light. The target material used to measure heat transfer was varied between water and aluminum. Temperature was recorded by one team member in a notebook every designated time interval while the second team member manually adjusted the dish to provide optimum focal point

Figure 44 Setup for Black painted glass jar testing

exposure to the target material.

Initial tests were set up to use a black painted glass jar as the target. However, the heat flux was intense enough to break the glass jar. Subsequently an aluminum plate was used as the testing target. The replacement target was a thin sheet of Aluminum 24cm x 11.2cm x 1.75mm spray-painted black. Because metal is a better conductor of heat than glass or water, the team was more confident that this target would yield a more uniform temperature distribution across its surface area than the jar. This allowed more confidence in the accuracy of convection loss calculations, which assumed a uniform temperature for the entire target. Instead of immersing a thermocouple in water, the setup involved pinching the tip of the thermocouple between a scrap aluminum block and the target plate. This non-adhesive setup was the most effective option because any tape used to attach the thermocouple would have quickly melted.

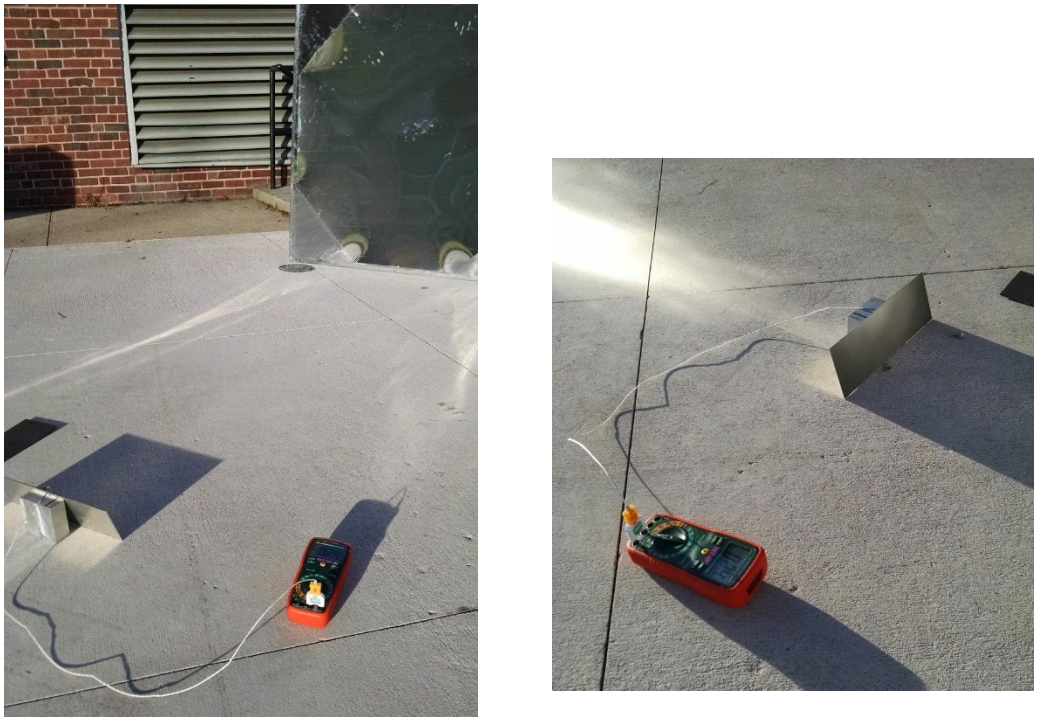

Figure 45 Test setup for aluminum plate

Temperature measurements were converted into retained energy using the mass and specific heat of the 6061 Aluminum target plate. Energy was taken to be zero at the initial temperature. The retained power was calculated by dividing the change in energy between temperature measurements by the measurement interval. Convective losses over the entire target were calculated using the equation for laminar flow over a flat plate. The total power absorbed was assumed to be the sum of the convective losses and the retained energy. The black paint, a non-ideal absorber, was estimated to have a 95% absorptivity. Therefore the calculated solar power was divided by 0.95 to determine the ideal solar power reflected by our dish.

3.5 Tracking Capabilities

With the focus on solar energy as a possible source of heat for the Stirling engine, it was acknowledged that the tracking of the sun was a major component of this idea being viable. As the sun moves through the sky the parabolic mirror needs to be directed to the position of the sun. A manual adjustment of the mirror was done for the beginning portion of this project, but it was later decided to automate the positioning of the mirror. This would make the mirror more efficient in its solar collection, require less maintenance of the mirror throughout the day, and prove the commercial application of this energy option, as seen in Figure 41 on page 75.

3.5.1 Position of the Sun

The azimuth angle and the elevation (altitude) angle are the two angles involved when tracking the sun. The azimuth angle is the sun's angle relative to the north vector, and the altitude angle is the sun's angle relative to the horizon. Both are measured in degrees, and change throughout the day. Figure 46 is a depiction of these angles. In the figure, the sun would be the point labeled "star" and the parabolic lens would be the point labeled "observer."

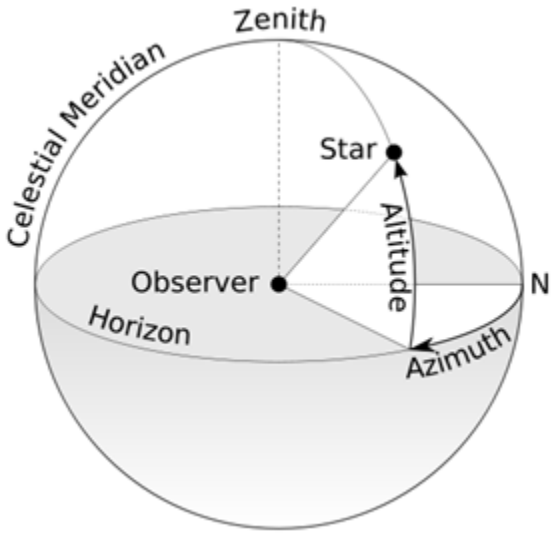

Figure 46 Depiction of following the sun

Both the azimuth and altitude angles can be determined by the latitude of the observer, the day number, and the time of day. The equations for the azimuth and altitude angles can be found below and their values are represented by the variables Φ and β respectively.

$$sin\beta = cosLcos\delta cosH + sinLsin\delta$$

$$\sin\phi = \frac{cos\delta sinH}{cos\beta}$$

where,

$L = Latitutde\ (degrees)$

$H = hour\ angle\ (degrees)$

$\delta = solar\ declination$

The hour angle is the number of degrees that the earth must rotate before the sun will be directly over one's local meridian. It is a simple calculation based upon the assumption that the earth rotates 360 degrees in 24 hours, so it rotates at 15 degrees per hour. It can be seen below.

$$H = (\frac{15°}{hour}) \cdot (hours\ before\ solar\ noon)$$

Solar declination can be found using data tables found in the annual publication of the American Ephemeris and Nautical Almanac, or through an equation that approximates the angle. With these equations the exact position of the sun can be found at any time of the day.

$$\delta = 23.45\sin\left[\left(\frac{360}{365}\right)(n - 81)\right]$$
$$n = \#\ of\ day\ in\ the\ 365\ \ year$$

3.5.2 Automation of the Reflector

A microcontroller known as the Raspberry Pi (RPi) was supplied by the project advisor along with two DC electric motors. The intention was to program the RPi to control the motors that would be integrated with the reflector frame. The RPi was programmed using Python. The

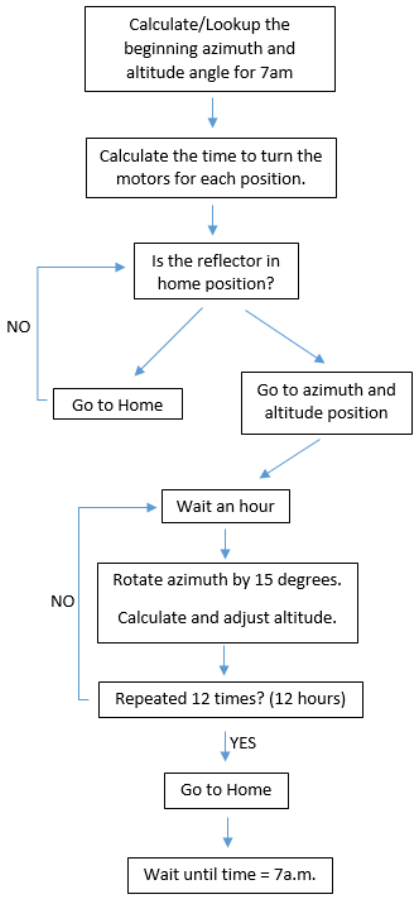

Figure 47 Tracking Algorithm

original concept for the tracking of the sun was to use four photosensitive resistors in order to sense the strongest source of light (the sun) and track it in accordance to the strength of the light. This would make the program dependent upon an analog source, and could lead to a few problems. First, the sun could be under cloud cover and throw off the sensor's tracking. Second, the RPi did not have enough analog input pins, so modifications would be needed to read all four sensors. The alternative to this was then to have the RPi either calculate or look up the exact location of the sun based upon the latitude, the date, and the time. This would then allow the tracker to avoid cloud interference, and make the process precise. The original idea for an algorithm devised to automate the reflector off of this idea can be seen below in Figure 48.

3.5.3 Current Components and Program

Due to time constraints, this full algorithm was not carried out. The control of three DC motors has been demonstrated to work. Currently the motors are programed to go through a

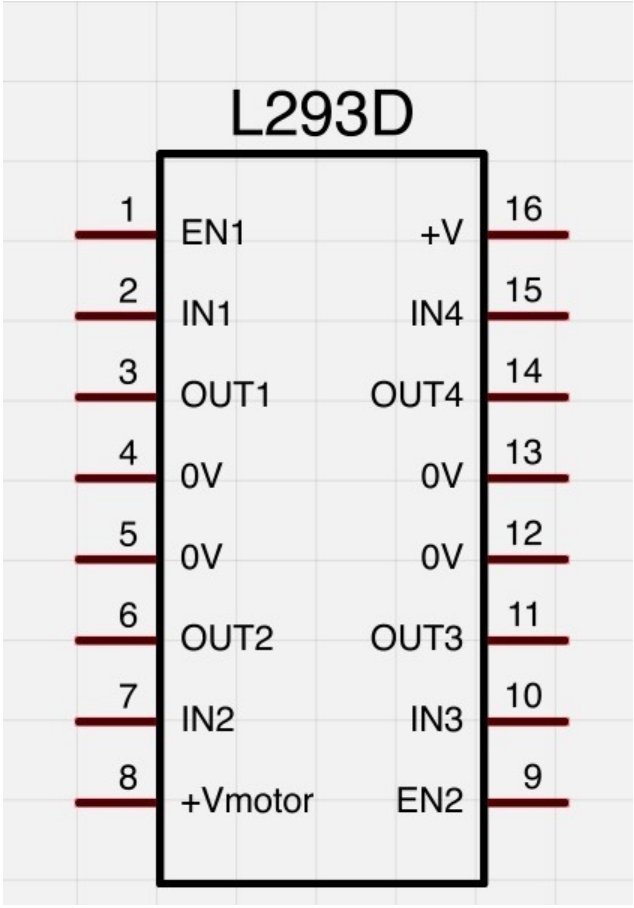

Figure 48 Motor Control IC chip

mock motion that can demonstrate the idea of how the automation will function. The motors are being controlled by an H-Bridge IC chip known as the L293D whose pinout can be seen below. These IC's can control the direction of a DC motor and the speed of the motors, and can control up to two motors per IC chip.

The DC motors given to the team came with a gearbox to increase the motor's torque, while also decreasing RPM. The motors currently run at about 80 RPM with a 12v power source and have an internal resistance of 17Ω. This gives a current less than 1 amp, which is within the operating tolerances of the IC chip.

A few motor control options were considered. Stepper motors, which are controlled by having an input designate a set amount of steps to take for a certain amount of degrees of movement, but also run hot as they are always on. Servo motors are used to get an exact position and are controlled by both an input to a set position and feedback from the motors, but are very expensive. Or, a DC motor, which has no feedback but a set RPM that can be timed to reach the desired position. These also have higher amounts of torque for less money, which was preferred. This project goal was to be cost effective and the DC motors could do what was needed with little cost. An equation was derived to determine the time the DC motors needed to be turned on for the needed rotation on the base, which can be seen below.

$$t = D * d * \frac{\theta}{360} * motor\ RPM * (\frac{60\ seconds}{1\ minute})$$

where: t = time in seconds , D = distance between the driven wheels, d= the diameter of the driven wheels , θ = angle needed to move, and the lengths are in the same units.

The plan was to have the panel go to a set elevation and start azimuth angle, and then rotates the azimuth 15 degrees every hour. The state of the automation will be discussed in Chapter 4.

Chapter 4: Results

The final engine and supporting electrical system in its housing is depicted in Figure 49.

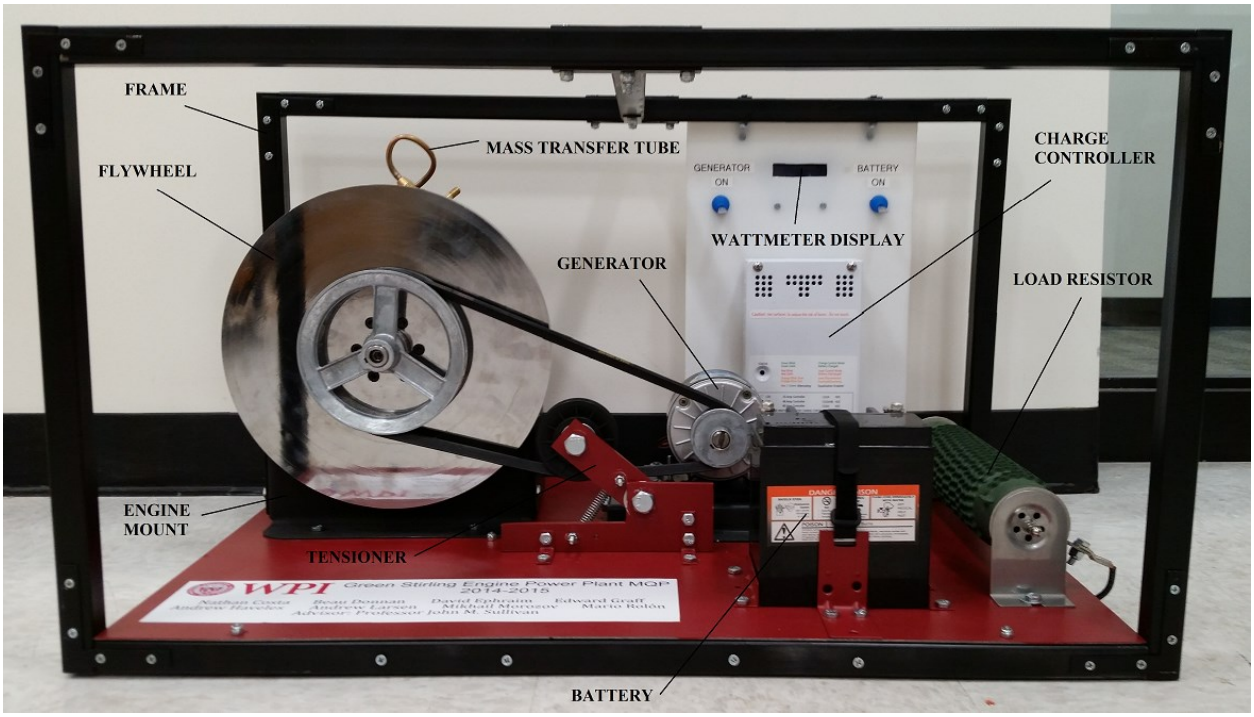

Figure 49 Final Project Assembly

4.1 Engine Improvements

The original design proved to have many flaws. The team designed, manufactured, and installed many parts that would improve the engine's performance. A new mass transfer tube was designed that connected the hot side cylinder to the cold side cylinder. At the same time, new engine heads were designed and manufactured. The wear and tear on the head gaskets due to repeated assembly and disassembly lead to manufacturing of new head gaskets. The original flywheel did not possess the moment of inertia necessary for the engine, and a new one was designed and manufactured. The crankshaft was modified to accommodate a rear bearing to reduce the friction.

4.1.1 Mass Transfer

In an alpha-type Stirling engine, the working fluid is transferred from one cylinder to the other through a tube connecting both sides, called a regenerator. As the fluid expands and contracts with the addition and subtraction of heat, it is transferred from one cylinder to the other through the tube. The engine works solely on the expansion and contraction of a fluid. Dead space created by the mass transfer tube can be detrimental to the performance of the engine. Because of this, the team redesigned the regenerator to be significantly smaller and shorter.

4.1.2 Heads

The team designed two new heads for the existing engine with properly sized holes for fitting a 1/8th ID copper tube in each side. The cold side head was designed with fins and a place to mount an 80mm computer fan in order to help dissipate heat. The hot side is simply an aluminum plate with the pipe fitting built in. A CAD model of the cold head can be seen below in Figure 50.

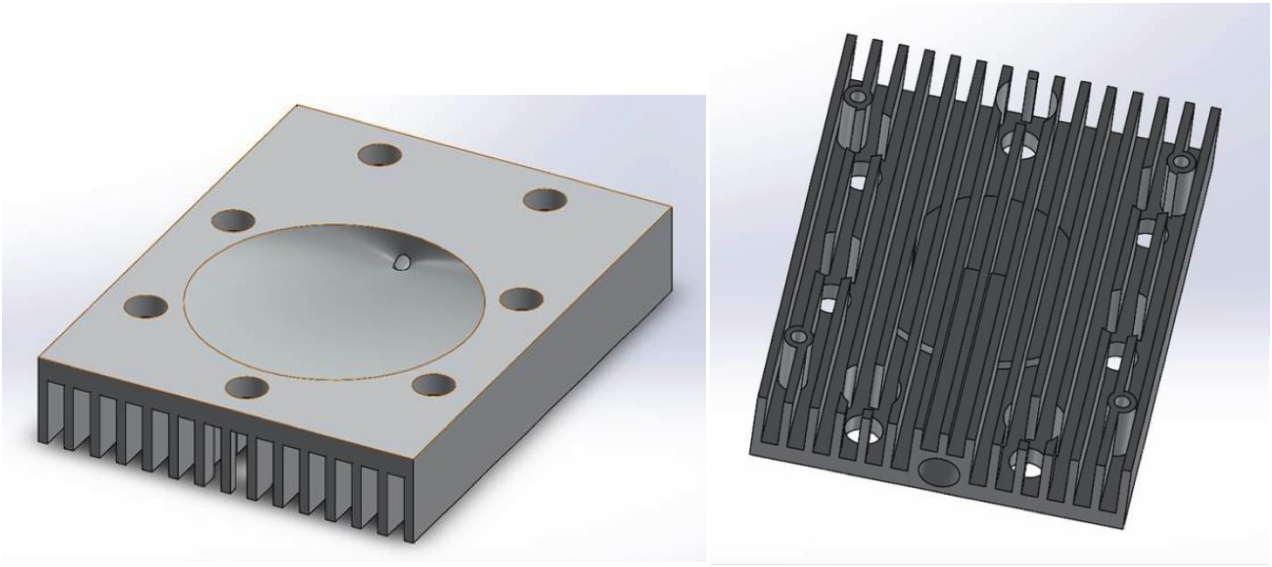

Figure 50 Cold Side Engine Head

The divots seen on the underside of the heads each have a surface area of 4.367 in^2 and add a dead volume of 0.2185 in^3. The next steps in this design were to machine the new heads and assemble them with the tubing and purchased fittings.

4.1.3 Gaskets

The original head gaskets were bent and did not hold pressure, so it was decided to manufacture new gaskets. A major challenge was to manufacture gaskets that would seal the engine while still being able to handle the potential operating temperatures upwards of 400 ℃. Most of the materials researched were not made for high temperature applications and therefore deemed unusable. Materials tested included laminated vermiculite-core carbon steel, copper, silicone, and binder free graphite.

Figure 51 Ground down engine-to-head surface

While testing the proposed gasket materials, it was noticed that the mating surface of the engine block had a poor sealing profile. To fix the poor profile and enable the gasket material to seal, the engine to head surface was surface ground until all damage present was removed.

It was determined graphite would satisfy the requirements. Although graphite is fragile, it conformed well to contacting surfaces while under pressure. The gaskets were tested and held at 90 psi for ten minutes and no leaks were discovered when using a bubble solution. The graphite has a temperature rating of 450 ℃. The major disadvantage of the graphite material is that it begins to fall apart with multiple installations and removals of the heads and new gaskets had to be fabricated. Of the tested materials, graphite was the only to meet all required specifications.

Figure 52 Graphite Gasket

4.1.4 Flywheel

A flywheel was constructed to even out the speed variations of the engine by storing kinetic energy during times of increased speed and releasing kinetic energy during times of reduced speed. The method for the computation of the needed moment of inertia for the flywheel can be found in the methodology section. After the addition of the flywheel the engine behaved much more smoothly over the course of a crankshaft revolution. Before the flywheel was installed, the engine would lurch to a stop during attempts to start the engine and the crankshaft would usually stop in approximately the same angular position. After the flywheel was added the engine would slowly coast to a stop after being spun.

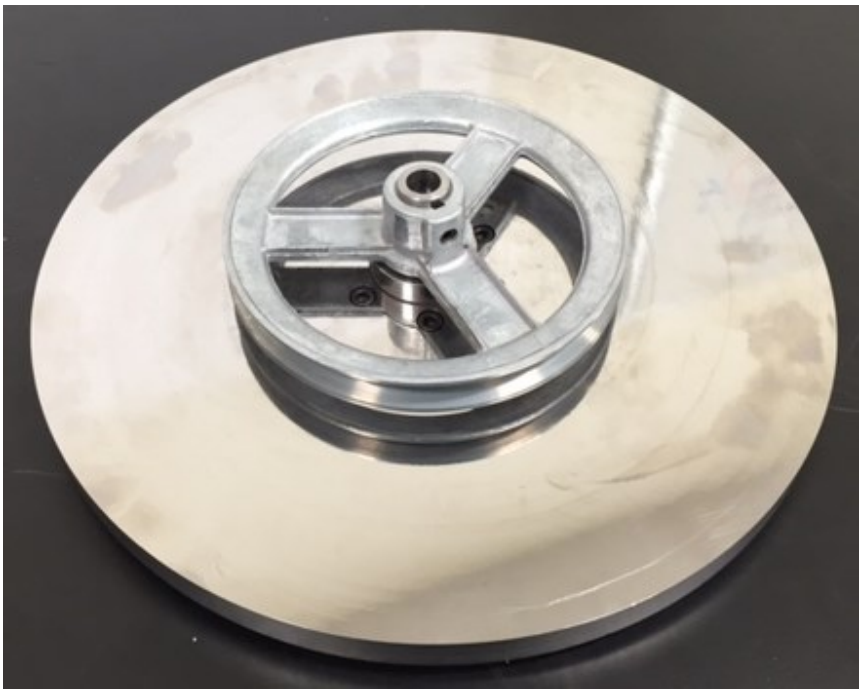

Figure 53 Finished Flywheel

4.1.5 Overall Engine Performance

Once the team removed all possible friction and the engine did not run it was decided that the surfaces on the interior of the engine should be altered in order to get more energy to the working fluid. Since the engine is designed to operate at upwards of 300℃ - where radiation becomes a factor, two major surface changes were tried and tested. The first change was the roughing up of the inside of the heads in order to increase the emissivity of the material along with shining the pistons to increasing their reflectivity. The second change was to blacken the heads to further increase their emissivity. The results are seen in Table 3 below:

Baseline - No Icewater				
	T_hothead [°C]	T_hotgas [°C]	T_coldgas [°C]	Delta T [°C]
After 1 min run	Approximately 350-400	250	110	140
After 2 min run		260	140	120

Pistons shined and Heads roughened up - Icewater				
	T_hothead [°C]	T_hotgas [°C]	T_coldgas [°C]	Delta T [°C]
After 1 min run	Approximately 350-400	230	70	160
After 2 min run		235	90	145

Blackened Heads - No Icewater				
	T_hothead [°C]	T_hotgas [°C]	T_coldgas [°C]	Delta T [°C]
After 1 min run	Approximately 350-400	227	154	73
After 2 min run		N/A	N/A	N/A

Table 3 Data from Engine Runs

Focusing on the Temperature of the hot gas, it can been seen that the changes made to the surfaces did not increase the temperature.

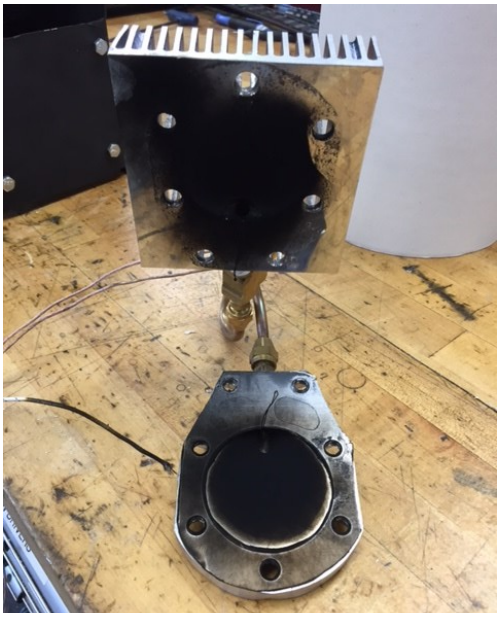

Figure 55 View of inside the engine heads after being blackened

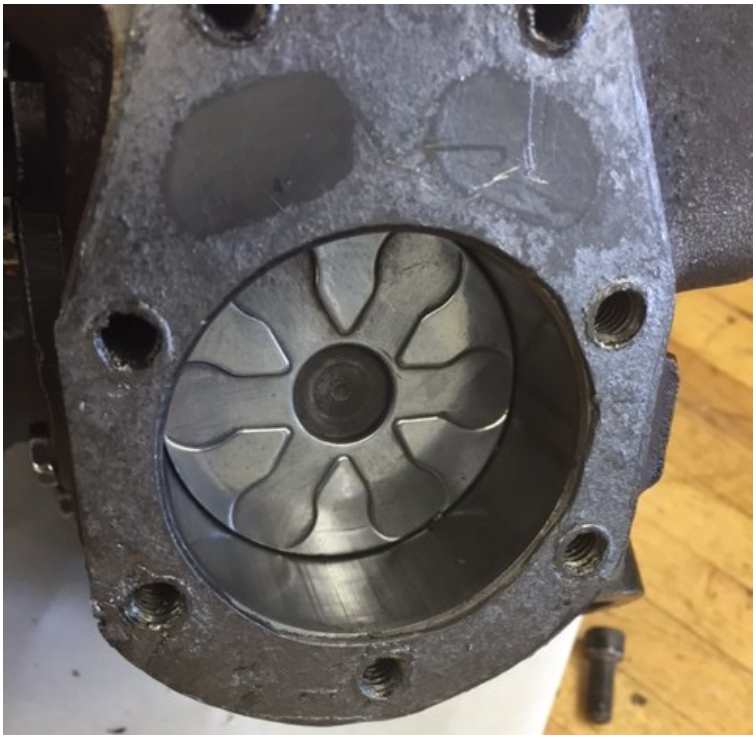

Figure 54 The top surface of a piston after being shined

4.2 Energy Transfer Components

The purpose of this section is to outline the performance testing of the electrical components of this project, including the generator, charge controller and wattmeter.

4.2.1 Generator

In order to analyze the power output of the generator, several tests were performed, involving spinning the generator at varying speeds with a power drill and measuring the electricity produced. For the purpose of connecting the generator shaft to a drill chuck, a custom fixture was designed and fabricated. Figure 56 depicts the configuration used.

Figure 57 Generator Shaft Adapter

To measure the electrical output of the generator, a resistor and two multimeters were used to close the circuit between the generator's wires. The circuit configuration is shown in Figure 58 below:

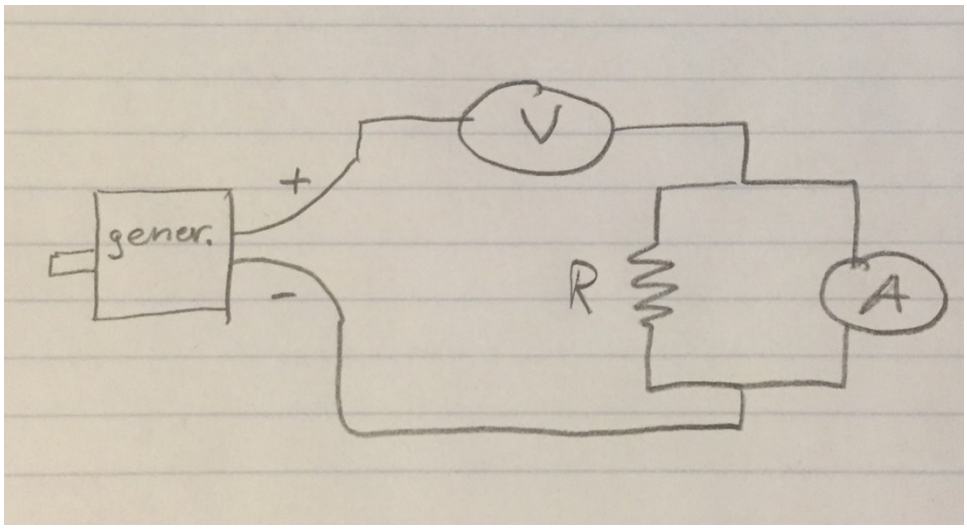

Figure 58 Generator schematic

Two sets of tests were initially performed—one with a 510 ohm resistor and one with a 111 ohm resistor. Measurements of the voltage and current in the circuit were recorded at 100 RPM increments up to 800 RPM, as well as a single test run at max drill speed (approximately 1300 RPM). Next, the current was multiplied by voltage to find power output of the generator. The results are shown in Table 4 below, with a graph of the power curves shown in Figure 59.

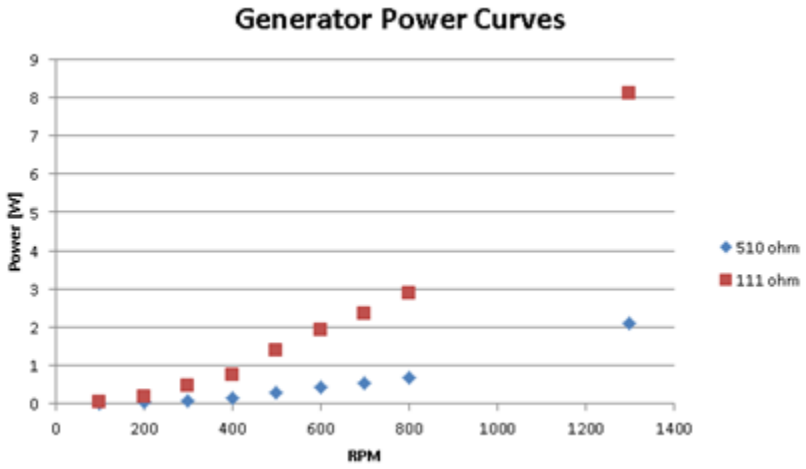

Figure 59 Generator Power Curves

	510 ohms			111 ohms		
RPM	current [mA]	voltage [V]	power [W]	current [mA]	voltage [V]	power [W]
100	5	2.5	0.0125	22.4	2.4	0.05376
200	10	5	0.05	41.9	4.5	0.18855
300	13.3	6.7	0.08911	66.8	7.3	0.48764
400	17.7	9	0.1593	83.6	9.1	0.76076
500	24.1	12.1	0.29161	112.3	12.4	1.39252
600	29.5	14.9	0.43955	132.1	14.6	1.92866
700	33.3	16.7	0.55611	146.2	16.2	2.36844
800	37.4	18.8	0.70312	160.7	17.9	2.87653
1300	64.6	32.5	2.0995	260	31.2	8.112

Table 4 Generator's Voltage, Current and Power, as a function of RPM

In order to better understand the relations between power output, RPM, and resistance values, the above experiment was repeated several more times with different resistors and different drill speeds. Figure 61 and Figure 62 illustrate this data:

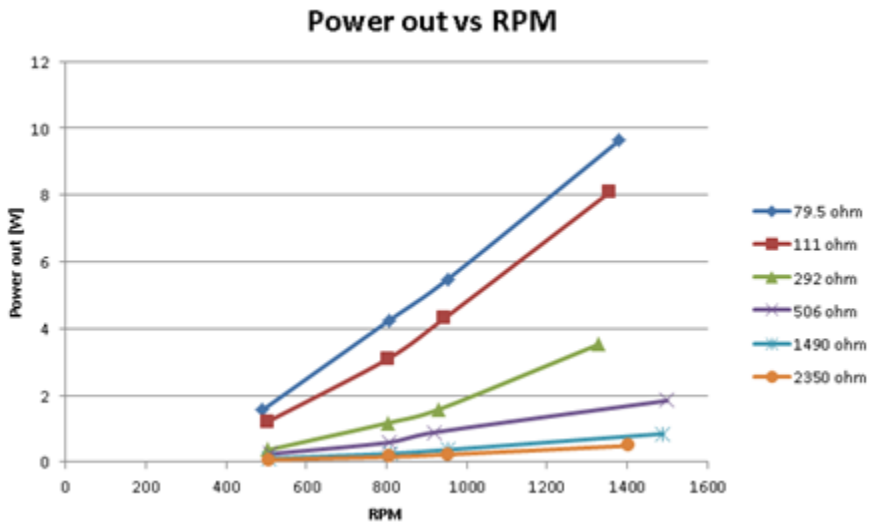

Figure 60: Generator Power Out VS Resistance

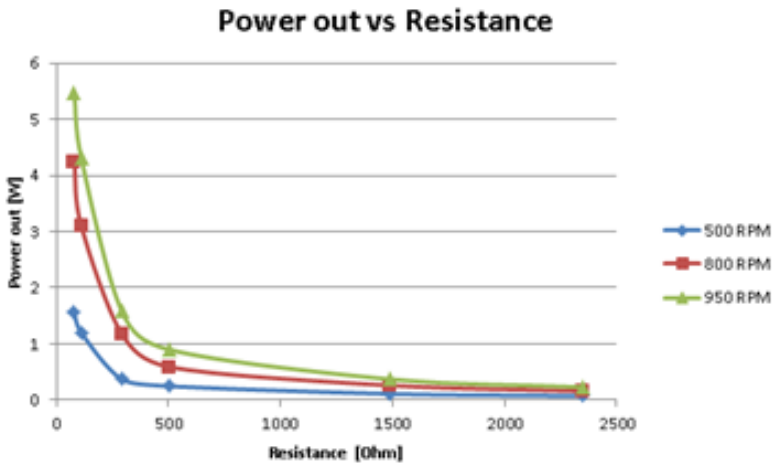

Figure 62 Generator Power out vs RPM

Since all the power values measured so far were very low, the test was repeated again with a 1 Ohm power resistor rated for 200 Watts, and a large capacitor to smooth out fluctuations from the current readings. For this test, a CNC mill was used to spin the generator due to the ease and accuracy of selecting spindle speed. An illustration of the test setup and circuit are shown in Figure 63.

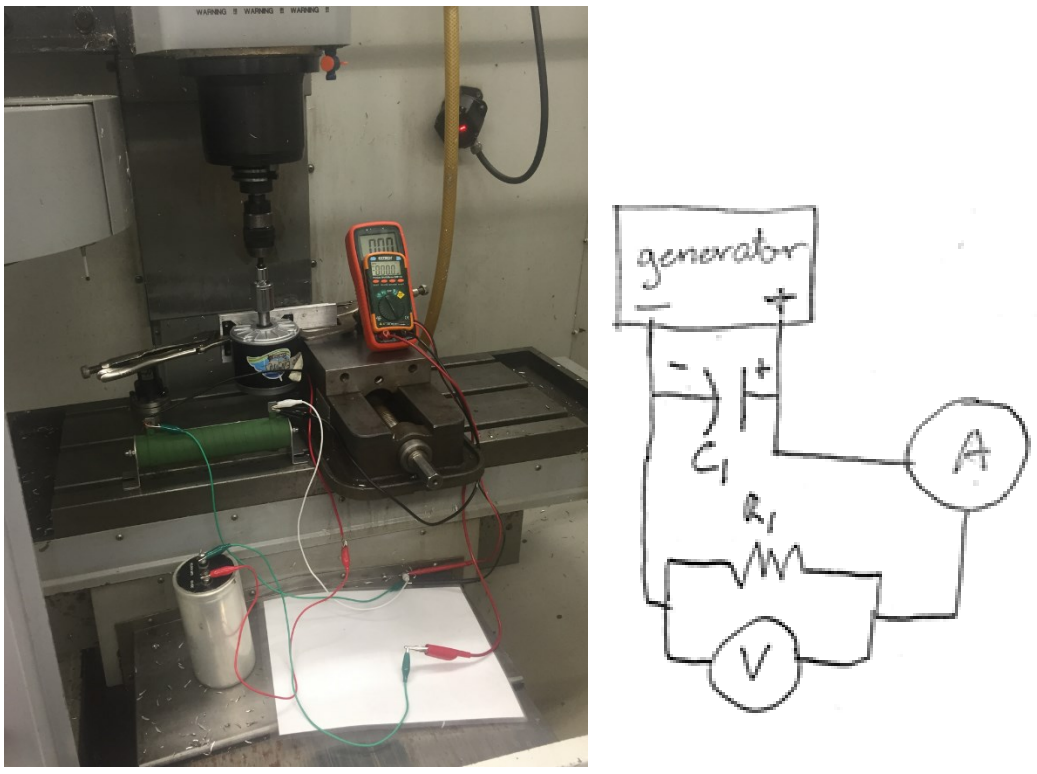

Figure 63 Generator Testing Setup

The power output was measured at 8 different speeds, ranging from 800 RPM to 2200 RPM at 200 RPM intervals. While the generator was spinning, the current and voltage through the resistor were measured simultaneously, then multiplied in order to calculate power output. The resulting power curve can be seen below in Figure 64.

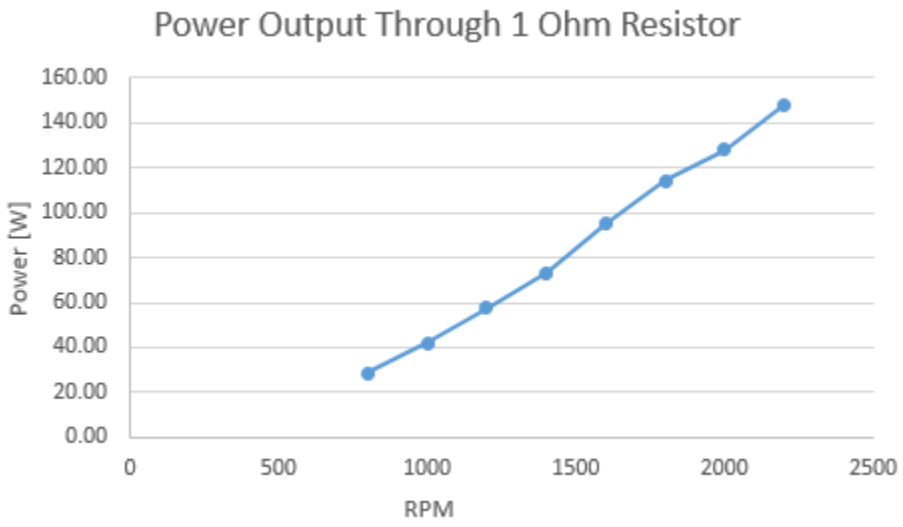

Figure 64 Generator Power Output through a 1 Ohm Resistor

The limiting factor of this test was the 1 Ohm resistor rated for 200W. At power outputs of over 100W, the resistor heated up very quickly. The resistor was allowed to cool down to room temperature in between tests, however for an actual engine test, the generator would be spinning for much longer than a few seconds, which would correspond to much more heat passing through the resistor, potentially damaging it. The Navy Electricity and Electronics Training Series states that a safety factor of 50% should be used for power ratings of electrical components (Jones, 1998). In order to safely dissipate 200W of power through a resistor for any extended period of time, that resistor should be rated for at least 300W. To allow room for increasing power outputs and error, a 1 Ohm 1kW resistor was purchased. This resistor was used

for all subsequent testing, and as a diversion load for the charge controller. The array of resistors used in testing can be seen in Figure 65, with the newest resistor on the right.

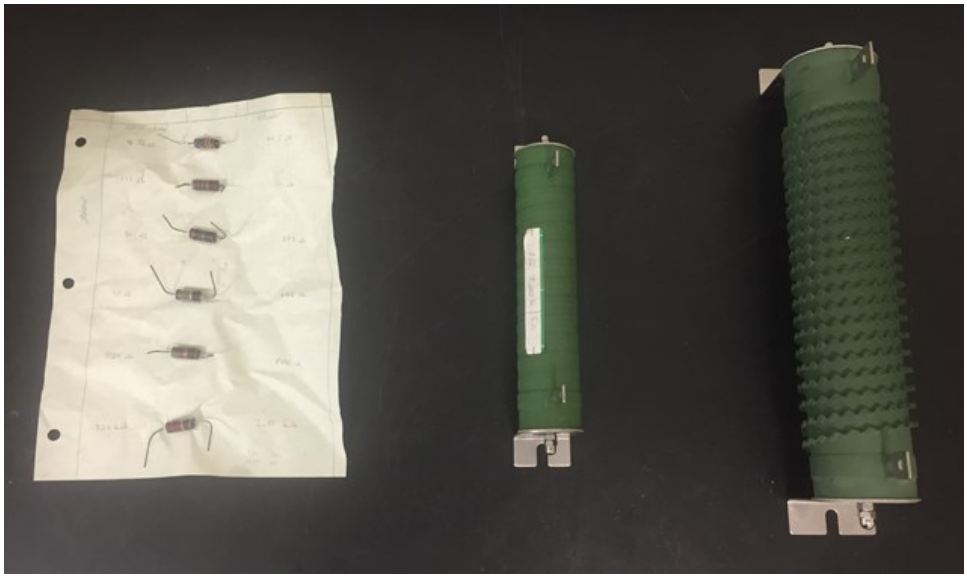

Figure 65 Resistors used

In order to measure the effect of charging a battery with the generator, as compared to dissipating electrical power through a resistor, some additional testing was performed. The generator was turned at varying speeds with a CNC mill, the electrical power was measured with a wattmeter, then passed into the battery. Since the positive and negative terminals of the generator and battery were connected directly, the battery had a tendency to spin the generator. In order to block the flow of electricity from the battery to the generator, a blocking diode was purchased and installed. This test configuration is shown in Figure 66.

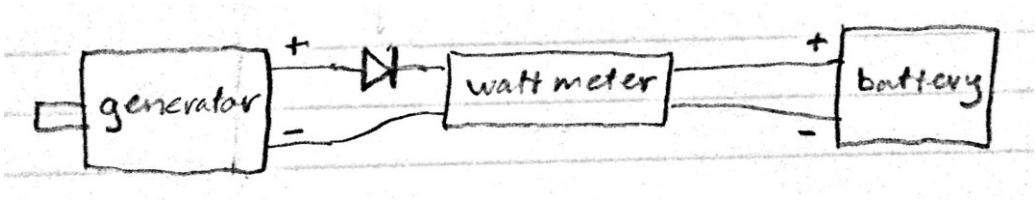

Figure 66 Battery charging test setup

For this test, the generator was spun at an initial speed of 1000RPM, which was increased gradually by 200RPM intervals, until it reached 2400 RPM. The power output readings from the wattmeter were recorded and plotted. Figure 67 illustrates this information.

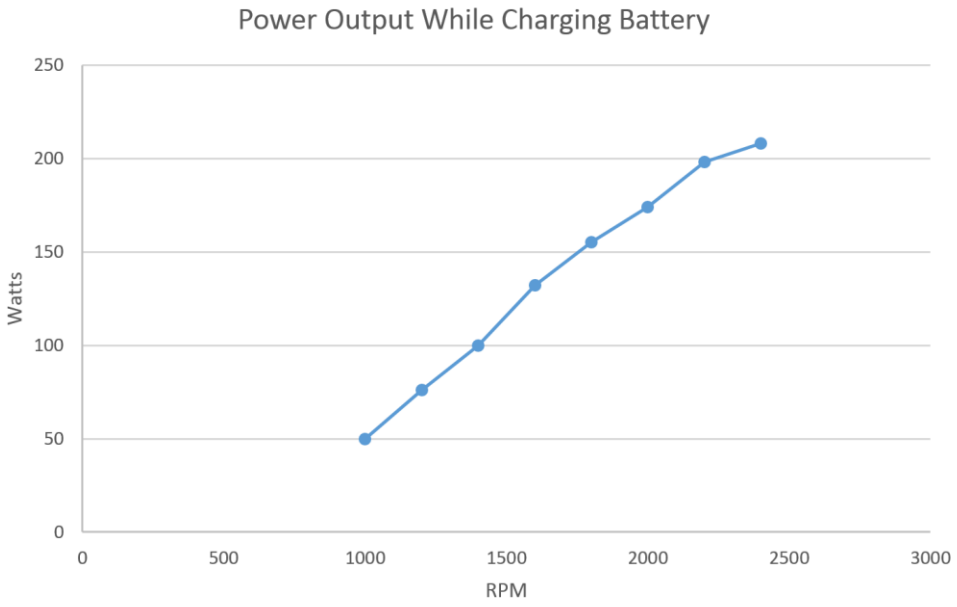

Figure 67 Charging Power vs RPM

4.3 Solar Power

This section covers the outcomes and interpreted results from the conducted solar tests. Tracking capabilities were explored and analyzed.

4.3.1 Parabolic Dish

Four tests were performed using the dish and target plate. The starting time of the test was used to interpolate energy data from the plot in Figure 43. Tests usually lasted no longer than 15 minutes. Wind gusts frequently caused the measured temperature to drop and because no wind data was recorded in real time, data was adjusted to provide a more idealized measurement with constant wind speed. The adjustment procedure simply involved removing outlier data in which the temperature fell from its previous peak due to wind gusts. The final product was a

smooth curve that plateaus at its peak temperature and had a duration between 3.5 and 5.5 minutes.

The average wattage during tests adjusted to the noontime peak of solar collection was 527W. Some notable measurements included a 269W average during a test conducted at 2:54PM, which was extrapolated to be 660W at noon. During a test begun at 1:49PM, a maximum temperature of 425^0C was measured. This test proved the dish's feasibility in powering the Stirling engine assuming a required 400^0C temperature differential. Another measurement of interest was a maximum wattage of 930W in which the temperature of the plate rose 100^0C over a 15-second interval.

Although the wooden frame measured 2305 in², the octagonal portion only encompassed 1604 in², or 1.03464 m². A larger parabolic dish built as an up-scaled version could therefore be expected to reliably supply the engine with 510W per square meter of parabolic area. The previous team reported that the average power supplied by the Fresnel lens was 130W with their 0.76 m² area. In reviewing the data of the previous team, however, it was discovered that the Fresnel dimension was actually 0.69 m² as they had neglected to subtract the wooden frame from the total lens area. Their effective power per area figure is then 194 W/m².

If the data from both teams is correct, then in conclusion, the parabolic dish was 163% more effective than the Fresnel lens per unit area. However, it is important to note that because test materials and assumptions were significantly different from those of the previous team, the percentage is considered theoretical.

4.3.2 Solar Tracking Capabilities

The motor control worked and the Raspberry Pi was a great way to control the motors, three motors were controllable by the L293D IC chips. The current was no problem for the motor controller, but a few issues did arise.

Mainly, the fitting of the motors onto the already designed solar reflector frame was an issue. The one motor that was implemented was mounted where the pinching rollers were originally designated to go. A roller was mounted onto the motor, and was able to hold the panel in place. The issue was that the motor spun too fast, and the spinning of the motor would initially pull on, and stretch the bungee cord, rather than instantaneously begin moving the panel. The panel would follow a moment after the motor began to turn. Then, when the motor stopped the panel would continue thru the movement due to the elasticity of the bungee cord. This would ruin the whole automation aspect because there is zero feedback on the exact position of the panel, and is rather blindly done by the program, which bases the panel's position off of timing of the motor's rotation. This is unreliable in a perfect scenario, and is completely unreliable in this current configuration. There was also an issue of the cord's fabric becoming worn due to the friction of the roller's surface. In Figure 68 the mounted motor can be seen.

Figure 68 Mounted Electric Motor

The other main issue with the automation, was the mounting of two motors on the base and its wheels. The design of the frame was made to be collapsible and so this took away from our ability to mount the motors. The motors would have to have been mounted in the area where the caster wheels were mounted, and the solar frame designers did not have the time to incorporate the motors into the current setup. The automation was not fully implemented, but there is enough evidence to support a major focus on automation in the next iteration of this project. This will be discussed in Chapter 5.

Chapter 5: Conclusions and Recommendations

5.1 Engine

As mentioned previously, the engine is incapable of maintaining operation. This is believed to be due to a lack of heat transfer between the heads and the working fluid. Looking at the temperature differences for the recorded attempts at operating the engine, it can be seen that the temperature difference between the heads and the working fluid is approximately the same as the temperature difference between the working fluid in each cylinder. Therefore, only one-third of the temperature difference between the heads is available for creating mechanical energy. This fact prevents the development of a great enough temperature difference, and therefore energy, difference between cylinders to overcome the effects of friction without heating the engine to the point where the internal clearances become too small and engines components start colliding.

Future groups should not use the existing engine to make a Stirling engine. The existing engine has been heavily modified and the project team feels that minimal improvements can be made to it. It is suspected that maintaining operation using this engine block would require the use of a large burner and significant cooling system, which precludes operating as an efficient green power source. It is suggested that future attempts at creating a green Stirling power plant create a new engine which has a large bore and short stroke.

5.2 Green Power Recommendations

The dish is inherently flawed. Ideally motors could be programed to track the Sun accurately and the reflect light onto the hot cylinder head without assistance. However, early iterations of the dish not shown in Chapter 3 could tailor to tracking and make the dish less susceptible to wind interference. The main structural difference is circular rails or tracks on

either side of the dish that would provide additional stability and offer superior mounting options for automation machinery. Design compressibility would need to be reevaluated.

The reflector does not hold a consistent vacuum in its current state. Leakage is a problem that was addressed by improving the pipe to frame interface seal and by applying a layer of paint to the back of the dish. Neither of these attempts succeeded in fully stopping the leak. Mylar is a thin, possibly porous, material and could be the primary source of the leak.

Finding an alternative method of creating a parabolic shape may be necessary. One potential solution is adhering a Mylar sheet to a fixed depth parabola. While a custom order dish would be costly, low cost options do exist. Dish shaped snow sleds similar to Figure 69 could serve as a fixed shape parabola.

Figure 69 Snow sled example

During the course of the project, there was concern that the reflected light from the parabolic dish would be unable to accurately focus on the engine head. A suggested solution was an independent mirror mounted on a stand to redirect the reflected light onto the engine head. The camera tripod in Figure 70 was purchased to serve as a portable stand for a redirection mirror. The mirror material needs must be able to withstand high temperatures, be durable, and

have a high reflectivity. Polished Aluminum was the most readily available material at the lowest cost that matched the criteria. However, this idea was never implemented.

Figure 70 Camera tripod for proposed mirror setup

5.2.1 Continuation into Automation of Solar Tracking

As was stated earlier, solar tracking can greatly increase the amount of solar energy collected and focused for our purposes. To completely optimize this process, 2 axis tracking will be needed, but this must also be incorporated into the design of the reflector. This was a major issue with our attempt to do so, and should be kept in mind while continuing this effort.

To make this possible while also keeping cost in mind, the use of the Raspberry Pi should also be incorporated, while also the design of the panel should be kept very light to keep motorization costs low. Some examples that can be found online of 2-axis solar trackers that use only two motors, which should be considered for the next design. The panel has on axis that falls right behind its center vertical axis, acting as its pivot axis to adjust azimuth, while the inclination is adjusted by one motor that adjusts that angle.

Other ideas that should be considered lie with the electronic information within the programming of this. The reflector should have feedback as to its position and the amount of light it is being exposed to. This information should all be recorded and can be used in the analysis of the solar collection. Also, an idea that was proposed initially was to have this solar tracking take into account, GPS location ad current date. This would allow for the most exact solar tracking and could be incorporated with the algorithm proposed in Chapter 3.

5.3 Energy Transfer and Storage Recommendations

The energy transfer and storage components generally worked as expected. The charge controller successfully regulated the current being sent to the battery, however, extensive testing was impossible to achieve because there was no electrical load to drain the battery. Future teams working on similar projects should consider implementing a larger battery bank which could be used to power lights at night before being recharged the next day. In an effort to utilize generated power as efficiently as possible, a more useful dump load could be used to dissipate excess power, such as a water heating element.

Bibliography

1. *30 kW Maintenance Free Stirling Engine for High Performance Dish Concentrating Solar Power*. (2010). Infinia. Retrieved from http://www1.eere.energy.gov/solar/pdfs/csp_prm2010_infinia_30kw.pdf

2. *Amazon*. Butterfly Photo. Web. http://ecx.images-amazon.com/images/I/41kkJdKOIvL._SY355_.jpg.

3. *Automatic Belt Tensioner*. (n.d.). Retrieved April 28, 2015, from http://www.aa1car.com/library/belt_tensioners.htm

4. Bumataria, R. K. & Patel, N. K. (2013). *Review of Stirling Engines for Pumping Water using Solar Energy as a source of Power.* International Journal of Engineering Research and Applications, Vol. 3, Issue 1, pp.864-868. Retreived from http://www.ijera.com/papers/Vol3_issue1/ED31864868.pdf

5. Chen, H., Czerniak, S., De La Cruz, E., Frankian, W., Jackson, G., Shiferaw, S., & Stewart, E. (2014). *Design of a Stirling Engine for Electricity Generation*. Worcester Polytechnic Institute. Retreived from https://www.youtube.com/watch?v=FyCLOXF1188

6. Cornwall, C., Horiuchi, A., & Lehman, C. (n.d.). NOAA Solar Position Calculator. Retrieved November 8, 2014, from http://www.esrl.noaa.gov/gmd/grad/solcalc/azel.html

7. *C-Series Multifunction DC Controller Owner's Manual*. (2003). Xantrex Technology.

8. Finkelstein, T. & Organ, A. G. (2001). *Air Engines: The History, Science, and Reality of the Perfect Engine.* New York: ASME Press

9. Hacsi, J. S. (2008). *Internal combustion engine with sidewall combustion chamber and method*. U.S. Patent 7387093 B2. Retrieved from http://www.google.com/patents/US7387093

10. *High Temperature Solar Thermal Technology Roadmap*. (n.d.). Wyld Group.

11. Iwaszko, J. R. (2011). *History of Wireless Electromagnetic Powered Flight*. AurumSolis Technologies. Retrieved from http://www.academia.edu/1917337/History_of_Wireless_Electromagnetic_Powered_Flight

12. Jadhao, S. & Mahantare, Y.V. (2013). *Literature review on Development of Stirling Engine*. Bapurao Deshmukh College of Engineering. Retrieved from http://www.academia.edu/7948428/LITERATURE_REVIEW_ON_DEVELOPMENT_OF_STIRLING_ENGINE

13. Jones, D. (1998). *Navy Electricity and Electronics Training Series (NEETS)* (pp. 127). Pensacola, FL: Naval Education and Training Professional Development and Technology Center.

14. Kontax Stirling Engines. (n.d.). Retrieved March 19. 2015, from http://www.stirlingengine.co.uk/History.asp

15. Manikeri, N. (2013). *Stirling Engine: A Complete Seminar Report on the Stirling Engine*. Retrieved from http://www.scribd.com/doc/129278031/stirling-engine#scribd

16. Mathas, C. (2014). *Slideshow: How NASA drives automotive technology – Part 1*. EDN Network. Retrieved from http://www.edn.com/Pdf/ViewPdf?contentItemId=4433686

17. Minassions, A. D. (2007). *Stirling Engines for Low-Temperature Solar-Thermal-Electric Power Generation.* Electrical Engineering and Computer Sciences, University of California at
Berkeley. Retreived from http://www.eecs.berkeley.edu/Pubs/TechRpts/2007/EECS-2007-172.pdf

18. Nightingale, N. P. (1986). *Automotive Stirling Engine: Mod II Design Report*. National Aeronautics and Space Administration. Retrieved from http://ntrs.nasa.gov/archive/nasa/casi.ntrs.nasa.gov/19880002196.pdf

19. Norton, R. (2012). *Design of Machinery: An Introduction to the Synthesis and Analysis of Mechanisms and Machines (5th ed.)*. New York: McGraw-Hill.

20. *Photovoltaics*. (2015). Murdoch University. Retrieved from http://www.see.murdoch.edu.au/resources/info/Tech/pv/

21. Rojas, D. (2015). *Green Power Science*. Green Power Science. Retrieved from http://greenpowerscience.com/index.html

22. Ross, A. (1993). *Making Stirling Engines.* Retrieved from http://zigherzog.net/stirling/literature/books/makingStirlingEngines-2.pdf

23. Saucers. *Flexible Flyer Sleds*. Paricon Inc. Retrieved from http://pariconsleds.com/index.php/saucers.html.

24. Sier, R. (2013). *Solar Dish Stirling Power Systems*. Retrieved March 22, 2015, from http://www.Stirlingengines.org.uk/sun/sola3.html

25. *Solar Maps*. (2009, February 1). Retrieved November 8, 2014, from http://www.nrel.gov/gis/solar.html

26. *Stirling Engine*. (n.d.). Stirling International. Retrieved April 3, 2015, from http://www.stirlinginternational.org/docs/presentations/history.asp

27. *Stirling Engine*. (n.d.). In Wikipedia. Retrieved November 16, 2014, from http://en.wikipedia.org/wiki/Stirling_engine

28. *Stirling engine as educational tool*. (n.d.). Stirlingshop.com. Retrieved March 21, 2015, from http://stirlingshop.com/index.html

29. Thombare, D.G. & Verma, S.K. (2008). *Technological development in the Stirling cycle engines.* Renewable and Sustainable Energy Reviews, 12, 1-38. Retrieved from http://www.academia.edu/3535256/Technological_Development_in_Stirling_Cycle Engine

30. *The Stirling Engine*. (n.d.). Electropaedia. Retrieved March 31, 2014, from http://www.mpoweruk.com/stirling_engine.htm

31. *V-Belt Tensioning*. (n.d.). Carlisle Power Transmission Products. Retrieved April 28, 2015, from http://www.c-rproducts.com/downloads/pdfs/guide_vbelt_tensioning.pdf

32. Vineeth, C.S. (2012). *Stirling Engines: A Beginner's Guide.* Retrieved from http://www.vineethcs.com/pdf/Stirling%20Engines-A%20Begineers%20Guide_rev_2.pdf

33. Walker, G. & Senft, J.R. (1985). *Lecture Notes in Engineering: Free Piston Stirling Engines*. Springer-Verlag Berlin, Heidelberg. Retrieved from http://download-v2.springer.com/static/pdf/48/bok%253A978-3-642-82526-2.pdf?token2=exp=1430353109~acl=%2Fstatic%2Fpdf%2F48%2Fbok%25253A978-3-642-82526-2.pdf*~hmac=3078642bc48ebe059c0a7749e55dcc2b15c9946ea407df4482c72c8f24ca8871

34. *WindZilla 12 V DC Permanent Magnet Motor Generator for Wind Turbine PMA*. (n.d.). Ebay. Retrieved April 28, 2015, from http://www.ebay.com/itm/WindZilla-12-V-DC-Permanent-Magnet-Motor-Generator-for-Wind-Turbine-PMA-/200716942488

35. *Your Guide to Renewable Energy.* (n.d.). Retrieved April 11, 2015, from http://www.renewable-energysources.com

Appendix

November 8th, 2:50PM	Time (Minutes)	Temperature (Celsius)	Energy (Joules)	Change in Energy	Power (Watts)	Side Convection Loss (Watts)	Face Convection Loss (Watts)	Absorbed Power (Watts)
Aluminum 6061	0	31	0	0	0	N/A	N/A	N/A
Volume (cm³)	0.5	100	7852.142592	7852.142592	261.7380864	[illegible]	[illegible]	[illegible]
47.04	1	[illegible]	[illegible]	[illegible]	[illegible]	[illegible]	47.117[illegible]	[illegible]
Density (g/cm³)	1.5	170	[illegible]	[illegible]	197.2[illegible]	2.57328	[illegible]	[illegible]
2.7	2	188	[illegible]	[illegible]	[illegible]	[illegible]	77.57787857	226.3415615
Mass (kg)	2.5	[illegible]	[illegible]	[illegible]	[illegible]	[illegible]	[illegible]	[illegible]
0.127008	2.75	221	21621.94192	[illegible]	[illegible]	[illegible]	91.64211887	278.6547183
Surface Area (cm²)	3	227	[illegible]	682.755[illegible]	45.5[illegible]	4.02864	94.25576160	[illegible]
[illegible]	3.25	230	[illegible]	341.397504	22.7598336	[illegible]	[illegible]	217.3[illegible]
Specific Heat Al (J/g°C)	3.5	250	24922.81779	2275.98886	151.732224	[illegible]	104.17[illegible]	504.5428576
0.896								AVERAGE WATTS:
Wind (m/s)								[illegible]
4.02[illegible]								MAXIMUM WATTS:
Temperature (Kelvin)								504.5428576
282							Avg. Possible Power (Watts)	Transmitted Power (Watts)
Length of Plate (cm)							[illegible]	[illegible]
24								
Area of Plate (cm²)								
[illegible]								
Dynamic Viscosity (kg/m*s)								
1.7500E-05								
Specific Heat Air (J/g°C)								
1.004[illegible]								
Thermal Conductivity (W/m*K)								
2.4[illegible]E-02								
Density Air (kg/m³)								
[illegible]								
Reynold's Number								
[illegible]								
Prandtl Number								
0.711								
Nusselt Number								
156								
Heat Transfer Coefficient (W/m²*K)								
16.1								
Heat Transfer Exterior Air (Watts)								
5.51								

Table 5 Collected Solar Data Nov 8th

November [illegible]	Time (Minutes)	Temperature (Celsius)	Energy (Joules)	Change in Energy	Power (Watts)	Side Convection Loss (Watts)	Face Convection Loss (Watts)	Absorbed Power (Watts)
Aluminum 6061	0	30	0	0	0	N/A	N/A	N/A
Volume (cm³)	0.25	[illegible]	[illegible]	[illegible]	[illegible]	[illegible]	[illegible]	[illegible]
47.04	0.5	85	[illegible]	[illegible]	[illegible]	[illegible]	[illegible]	[illegible]
Density (g/cm³)	0.75	105	[illegible]	[illegible]	[illegible]	[illegible]	[illegible]	[illegible]
2.7	1	[illegible]	[illegible]	[illegible]	[illegible]	[illegible]	[illegible]	[illegible]
Mass (kg)	1.25	[illegible]	[illegible]	[illegible]	[illegible]	[illegible]	[illegible]	[illegible]
0.127008	1.5	[illegible]	[illegible]	[illegible]	[illegible]	[illegible]	[illegible]	[illegible]
Surface Area (cm²)	1.75	[illegible]	[illegible]	[illegible]	[illegible]	[illegible]	[illegible]	[illegible]
[illegible]	2	[illegible]	[illegible]	[illegible]	[illegible]	[illegible]	[illegible]	[illegible]
Specific Heat Al (J/g°C)	2.25	[illegible]	[illegible]	[illegible]	[illegible]	[illegible]	[illegible]	[illegible]
0.896	2.5	[illegible]	[illegible]	[illegible]	[illegible]	[illegible]	[illegible]	[illegible]
Wind (m/s)	2.75	[illegible]	[illegible]	[illegible]	[illegible]	[illegible]	[illegible]	[illegible]
[illegible]	3	[illegible]	[illegible]	[illegible]	[illegible]	[illegible]	[illegible]	[illegible]
Temperature (Kelvin)	3.25	[illegible]	[illegible]	[illegible]	[illegible]	[illegible]	[illegible]	[illegible]
[illegible]	3.5	[illegible]	[illegible]	[illegible]	[illegible]	[illegible]	[illegible]	[illegible]
Length of Plate (cm)	3.75	[illegible]	[illegible]	[illegible]	[illegible]	[illegible]	[illegible]	[illegible]
24	4	[illegible]	[illegible]	[illegible]	[illegible]	[illegible]	[illegible]	[illegible]
Area of Plate (cm²)	4.25	[illegible]	[illegible]	[illegible]	[illegible]	[illegible]	[illegible]	[illegible]
[illegible]	4.5	[illegible]	[illegible]	[illegible]	[illegible]	[illegible]	[illegible]	[illegible]
Dynamic Viscosity (kg/m*s)	4.75	[illegible]	[illegible]	[illegible]	[illegible]	[illegible]	[illegible]	[illegible]
[illegible]	5	[illegible]	[illegible]	[illegible]	[illegible]	[illegible]	[illegible]	[illegible]
Specific Heat Air (J/g°C)	5.25	[illegible]	[illegible]	[illegible]	[illegible]	[illegible]	[illegible]	[illegible]
[illegible]	5.5	425	[illegible]	[illegible]	[illegible]	[illegible]	[illegible]	[illegible]
Thermal Conductivity (W/m*K)							Avg. Possible Power (Watts)	AVERAGE WATTS:
[illegible]							[illegible]	[illegible]
Density Air (kg/m³)								MAXIMUM WATTS:
[illegible]								[illegible]
Reynold's Number								Transmitted Power (Watts)
[illegible]								[illegible]
Prandtl Number								
0.711								
Nusselt Number								
[illegible]								
Heat Transfer Coefficient (W/m²*K)								
[illegible]								

Table 6 Collected Solar Data Nov 15th

November 19th, 2014 (1:02-1:27PM)	Time (Minutes)	Temperature (Celsius)	Energy (Joules)	Change in Energy	Power (Watts)	Side Convection Loss (Watts)	Face Convection Loss (Watts)	Absorbed Power (Watts)		
Aluminum 6061	0	21	0	0		N/A	N/A	N/A		
Volume (cm^3)	0.25	72	5803.757568	5803.757568	386.9171712	1.36752	37.21102154	462.7067343		
47.04	0.5	171	17069.8752	11266.11763	751.0745088	3.19704	86.99333404	928.2582171		
Density (g/cm^3)	0.75	200	20370.05107	3300.175872	220.0117248	3.73296	101.5760338	426.8967483		
2.7	1	230	23784.02611	3403.97504	227.598336	4.28736	116.661581	465.2088581		
Mass (kg)	1.25	245	25491.01363	1706.98752	113.799168	4.56456	124.2043657	366.7724894		
0.127008	1.5	280	29473.98451	3982.97088	265.531392	5.21136	141.8040632	554.3610783		
Surface Area (cm^2)	1.75	293	30953.3737	1479.389184	98.6259456	5.4516	148.3412346	400.7600146		
549.92	2	313	33229.35706	2275.98336	151.732224	5.8212	158.3982674	474.3499587		
Specific Heat Al (J/g*°C)	2.25	321	34139.7504	910.393344	60.6928896	5.96904	162.4210805	391.5040906		
0.896	2.5	325	34594.94707	455.196672	30.3464448	6.04296	164.4324871	365.2543789		
Wind (m/s)	2.75	329	35050.14374	455.196672	30.3464448	6.11688	166.4438936	369.3611121		
5.27778	3	334	35619.13958	568.99584	37.933056	6.20928	168.9581539	382.0586297		
Temperature (Kelvin)	3.25	336	35846.73792	227.598336	15.1732224	6.24624	169.9638651	361.3471727		
271	3.5	342	36529.53293	682.795008	45.5196672	6.35712	172.980965	397.8887172	MAX	POSS
Length of Plate (cm)								453.3827257	928.2582	462.5848
24	0	39	0	0	0	N/A	N/A	N/A		
Area of Plate (cm^2)	0.25	86	5348.560896	5348.560896	356.5707264	1.62624	44.25094453	446.6988655		
268.8	0.5	133	10697.12179	5348.560896	356.5707264	2.4948	67.88497173	494.8854699		
Dynamic Viscosity (kg/m*s)	0.75	191	17297.47354	6600.351744	440.0234496	3.56664	97.05036699	637.6908236		
1.75888E-05	1	208	19232.05939	1934.585856	128.9723904	3.8808	105.5988449	340.0508802		
Specific Heat Air (J/g*°C)	1.25	244	23328.82944	4096.770048	273.1180032	4.54608	123.701504	525.0670913		
1.004108	1.5	252	24239.22278	910.393344	60.6928896	4.69392	127.7243172	320.8854439		
Thermal Conductivity (W/m*K)	1.75	269	26173.80864	1934.585856	128.9723904	5.00808	136.2727951	406.5260606		
2.48288E-02	2	290	28563.59117	2389.782528	159.3188352	5.39616	146.8326796	458.3803544		
Density Air (kg/m^3)	2.25	318	31749.96787	3186.376704	212.4251136	5.9136	160.9125256	540.1637647		
1.293	2.5	323	32318.96371	568.99584	37.933056	6.006	163.4267858	370.7926236		
Reynold's Number	2.75	333	33456.95539	1137.99168	75.866112	6.1908	168.4553002	408.9675124		
9.31E+04	3	336	33798.3529	341.397504	22.7598336	6.24624	169.9638651	368.9337839		
Prandtl Number	3.25	347	35050.14374	1251.790848	83.4527232	6.44952	175.4952232	440.8926896		
0.711	3.5	351	35505.34042	455.196672	30.3464448	6.52344	177.5066298	391.8833443		
Nusselt Number	3.75	355	35960.53709	455.196672	30.3464448	6.59736	179.5180363	395.9798775	MAX	POSS
181								437.4462684	637.6908	425.4854
Heat Transfer Coefficient (W/m^2*K)										
18.7										

Table 7 Collected Solar Data Nov 19th

$\theta := 0, 0.001 .. 70 \frac{2 \cdot \pi}{360}$ Theta is the dish elevation angle

$b_1 := 24in$ a1 is front rope length

$c_1 := 24in$

$a_1(\theta) := \sqrt{b_1^2 + c_1^2 - 2 \cdot b_1 \cdot c_1 \cdot \cos(\theta)}$

$b_2 := 24in$ a2 is back rope length

$c_2 := 24in$

$a_2(\theta) := \sqrt{b_2^2 + c_2^2 - 2 \cdot b_2 \cdot c_2 \cdot \cos(\pi - \theta)}$

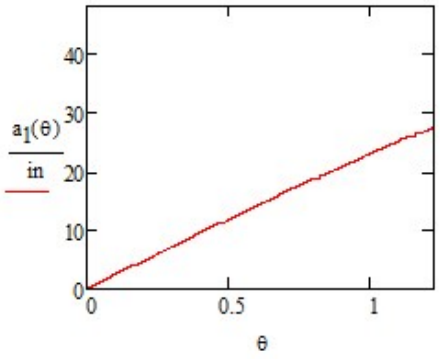

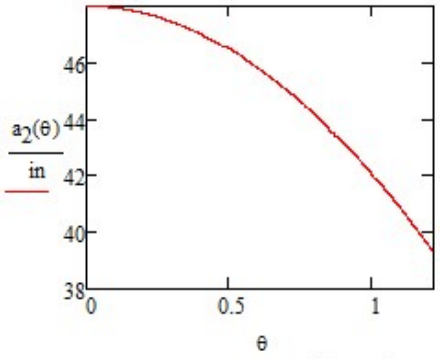

$a_1(0) = 0 \cdot in$ $a_1\left(70 \cdot \frac{2 \cdot \pi}{360}\right) = 27.532 in$

$a_2(0) = 48 in$ $a_2\left(70 \cdot \frac{2 \cdot \pi}{360}\right) = 39.319 in$

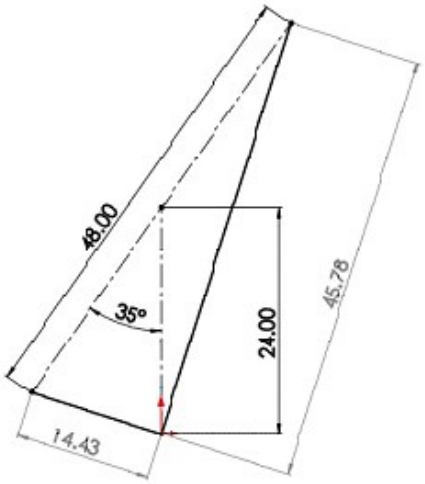

$a_3(\theta) := a_1(\theta) + a_2(\theta)$

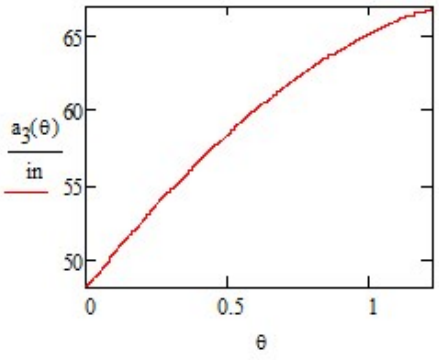

$a_3(0) = 48 in$ $a_3\left(70 \cdot \frac{2 \cdot \pi}{360}\right) = 66.851 in$

Figure 71 Early Design MathCAD Rope Length Calculations

$\theta := 0, 0.001 .. 70 \cdot \frac{2 \cdot \pi}{360}$ Theta is the dish elevation angle

$b_1 := 24in$ a1 is front rope length

$c_1 := 12in$

$a_1(\theta) := \sqrt{b_1^2 + c_1^2 - 2 \cdot b_1 \cdot c_1 \cdot \cos\left(\theta + \frac{11\pi}{36}\right)}$

$b_2 := 24in$ a2 is back rope length

$c_2 := 12in$

$a_2(\theta) := \sqrt{b_2^2 + c_2^2 - 2 \cdot b_2 \cdot c_2 \cdot \cos\left(\frac{25\pi}{36} - \theta\right)}$

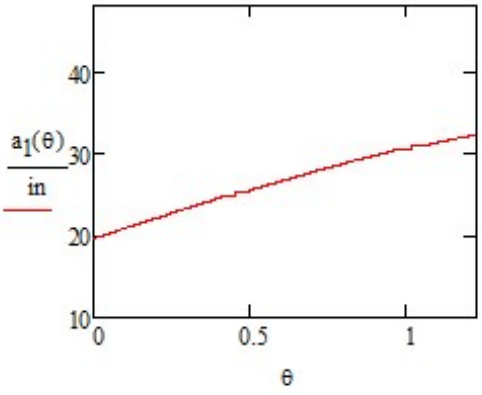

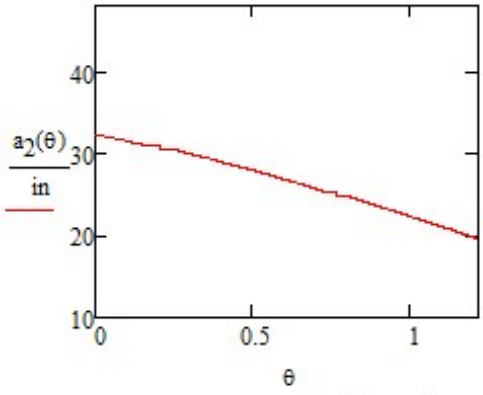

$a_1(0) = 19.739in$ $a_1\left(70 \cdot \frac{2 \cdot \pi}{360}\right) = 32.41in$

$a_2(0) = 32.41in$ $a_2\left(70 \cdot \frac{2 \cdot \pi}{360}\right) = 19.739in$

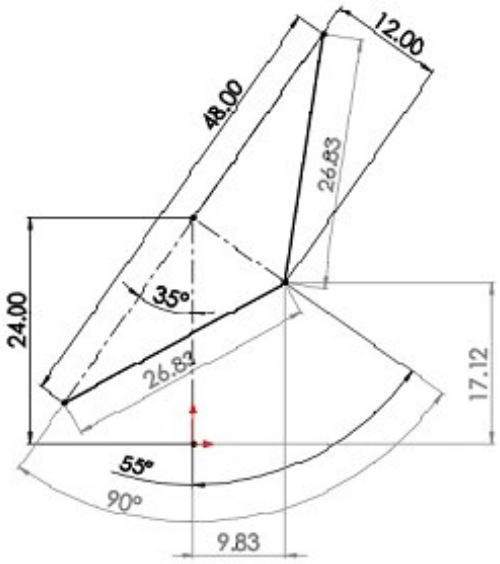

$a_3(\theta) := a_1(\theta) + a_2(\theta)$

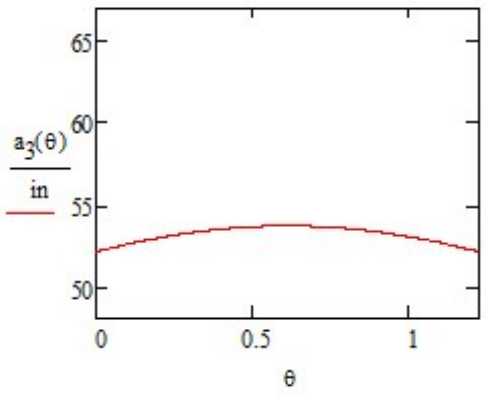

$a_3(0) = 52.148in$ $a_3\left(70 \cdot \frac{\pi}{360}\right) = 53.666in$

Figure 72 Final Design MathCAD Rope Length Calculations

$\theta_{1A} := 0 + \frac{11 \cdot \pi}{36}$

a1 is front rope length

$b_1 := 24in$

$c_1 := 0in, 0.001in .. 30in$

$a_{1A}(c_1) := \sqrt{b_1^2 + c_1^2 - 2 \cdot b_1 \cdot c_1 \cdot \cos(\theta_{1A})}$

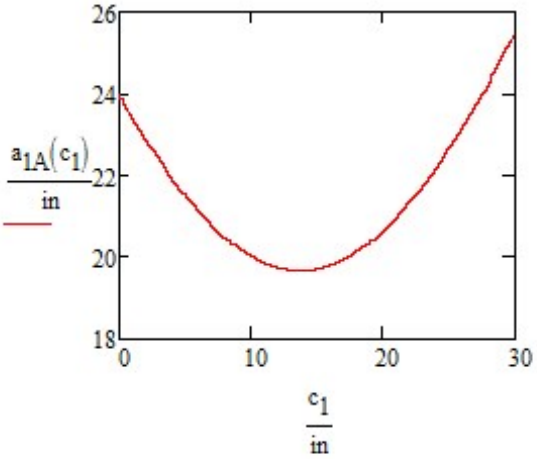

$\theta_{2A} := \pi - \theta_{1A}$

a2 is back rope length

$b_2 := 24in$

$c_2 := 0in, 0.001in .. 30in$

$a_{2A}(c_2) := \sqrt{b_2^2 + c_2^2 - 2 \cdot b_2 \cdot c_2 \cdot \cos(\theta_{2A})}$

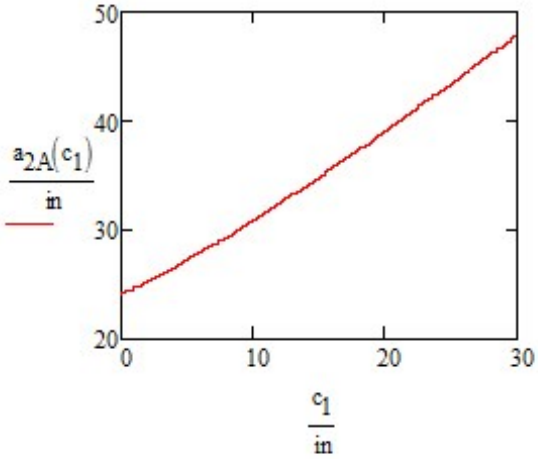

$\theta_{1B} := \frac{7 \cdot \pi}{36} + \frac{11 \cdot \pi}{36} = 1.571$

$a_{1B}(c_1) := \sqrt{b_1^2 + c_1^2 - 2 \cdot b_1 \cdot c_1 \cdot \cos(\theta_{1B})}$

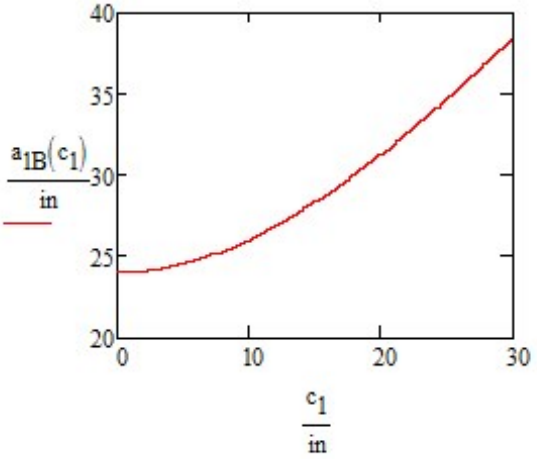

$\theta_{2B} := \pi - \theta_{1B}$

$a_{2B}(c_2) := \sqrt{b_2^2 + c_2^2 - 2 \cdot b_2 \cdot c_2 \cdot \cos(\theta_{2B})}$

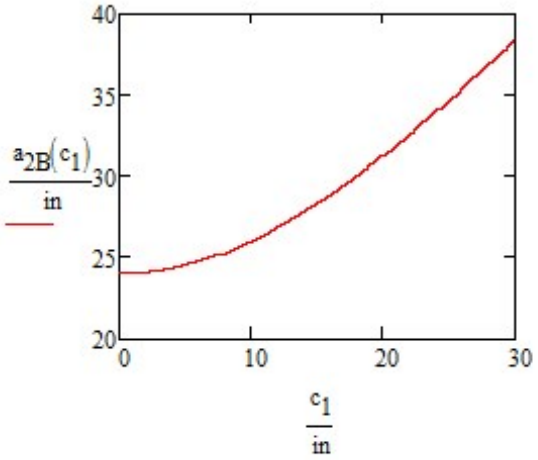

Figure 73 Final Design Elevation Change Calculations